Scientific Research Publishing

Modeling and Numerical Simulation of Material Science, 2026, 16(2), 15-44
https://www.scirp.org/journal/mnsms
ISSN Online: 2164-5353
ISSN Print: 2164-5345

Eliminating Residual Non-Binary Intensities in Pixelated EUV Source Optimization

Athanasios Batgidis[1], Eytan Barouch[1], Michael Yeung[2]

[1]Department of Mechanical Engineering, Boston University, Boston, MA, USA
[2]Fastlitho, San Jose, CA, USA
Email: eytanbrch@gmail.com

How to cite this paper: Batgidis, A., Barouch, E. and Yeung, M. (2026) Eliminating Residual Non-Binary Intensities in Pixelated EUV Source Optimization. *Modeling and Numerical Simulation of Material Science*, **16**, 15-44.
https://doi.org/10.4236/mnsms.2026.162002

Received: April 4, 2026
Accepted: April 27, 2026
Published: April 30, 2026

Abstract

Recently, pixelated source optimization (SO) for EUV lithography has been posed as a convex quadratic program (QP) whose decision variables are pupil pixel intensities. The result of this QP generated an almost binary illuminator (~95%), where optimal solutions are composed of pixels lying almost exclusively at the set boundaries (0 or 1), while a small subset remains strictly interior. Although these pixels are few, they complicate hardware realization and raise the question of whether they reflect intrinsic properties of the lithography system or are simply numerical artifacts. In this paper, we studied the stability of non-binary pixels in convex QP source optimization by systematically varying three parameters that directly affect the optimization scheme: the total source power constraint W, the placement of measurement point pairs used to form the objective function, and the numerical precision used to build and solve the QP. Using a primal-dual interior-point method (PDIPM) and high-fidelity aerial image simulation, we quantified non-binary intensities and examined how this metric changed under controlled perturbations of the problem statement. Across multiple test patterns and both circular and annular pixelated pupils, we observed that increasing W yields a noisy reduction in the number of non-binary pixels, consistent with increased constraint activity under a sum equality constraint. In contrast, varying measurement pairs led to non-monotonic changes in non-binary pixels without an underlying trend. We also showed that an equal number ($p = 100$) of point pairs placed randomly across trials yielded noticeably different optimal sources and aerial images, while preserving the same exact number of non-binary pixels. Finally, repeating identical optimization trials in 64-bit and 128-bit arithmetic yielded systematically fewer non-binary pixels in 128-bit while preserving identical illuminator shapes and aerial image metrics (NILS, line intensity) in both circular and annular illuminators. We also showed that manually rounding these intensities to the nearest integer value does not affect the aerial image in a

significant manner. These results indicate that non-binary pixels are the result of a numerically sensitive QP, and that higher-precision arithmetic primarily reduces active-set ambiguity rather than altering the physical optimum.

Keywords

EUV Lithography, Quadratic Programming, Source Optimization, Constraint Optimization, Numerical Precision

1. Introduction

Extreme Ultraviolet (EUV) lithography has been the state-of-the-art solution for advanced semiconductor manufacturing, offering sub-7 nm patterning capability. A central challenge in EUV lithography is the design of an optimal illumination source that ensures pattern fidelity, high image log slope (ILS), and minimal edge placement error (EPE). Pixelated source-mask optimization (SMO) offers a high degree of control over illumination profiles.

The earliest and most widely adopted approach to pixelated SO relaxes pupil pixel intensities from {0, 1} to the continuous interval [0, 1] and minimizes a smooth cost function, typically measuring the difference between the simulated and target aerial or resist image, using methods such as steepest descent, conjugate gradient [1]. More recent work has extended this framework to EUV and high-NA EUV systems, incorporating M3D effects. To recover a physically realizable pupil, these methods typically add a binary penalty term to the objective, which pushes pixel values toward 0 or 1 but trades off against imaging fidelity and introduces a user-selected weight parameter. As a result, the final source is rarely binary at convergence and must still be rounded, meaning binarity is *imposed* by the cost function rather than guaranteed by the optimization itself.

A second family of methods treats source optimization as a combinatorial search problem and applies genetic algorithms (GAs) or particle swarm optimization (PSO) to explore the space of pupil configurations without using gradient information [2]. Binary-coded GAs are particularly appealing for SO because each pixel is encoded as a single bit, so the feasible set is exactly the binary set; as such, non-binary intensities cannot arise by construction. More recent hybrids have been proposed mainly to escape local minima and accelerate convergence. However, these methods sacrifice reproducibility, since different random seeds produce meaningfully different sources, and they scale poorly as the number of pupil pixels grows.

Over the past few years, machine learning has been applied to SO and SMO, either by training a network to map target layouts directly to optimized sources or by embedding lithographic physics into a trainable architecture [3]. These methods almost universally produce continuous-valued pupil intensities in [0, 1] and rely on a fixed threshold (typically 0.5) as a post-processing step to recover a binary source, so the binarization problem is deferred rather than solved.

Recent approaches, such as the one proposed by Yeung and Barouch, use convex quadratic programming to derive a majority of binary illuminator points (pixels) [4]. Their method frequently produces a solution in which about 95% of pixel intensities are binary (normalized to 0 or 1), with the remaining few pixels showing intermediate values. This partial binarization is advantageous for system simplicity, thermal uniformity, and optical longevity, but the residual non-binary pixels raise both practical and theoretical concerns. In real-world hardware like DMD arrays or micromirror-based projection systems, truly binary outputs are strongly preferred for both simplicity of the system, but also reliability. Additionally, the presence of non-binary values might be symptomatic of numerical artifacts or insufficient solution convergence. Across all three families described above, binarity is either enforced by a penalty, encoded discretely at the cost of tractability, or deferred to a rounding step; the convex QP formulation studied here is unusual in that near-binary solutions emerge naturally from the optimum, which is what makes the residual non-binary pixels worth examining. Our methodology is focused on proving the existence of numerical imprecision, its effect on the pixelated pupil, and finally, the resultant aerial image.

2. Problem Formulation and Methodology

The source optimization will follow Barouch and Yeung's model, namely, a convex quadratic programming problem. We will briefly restate its formulation below:

Let ρ_i equal the intensity of pixel i in the illuminator. Let T_0 equal the threshold intensity. Then, the solution vector is defined as

$$\boldsymbol{q} = \left[\rho_1, \rho_2, \cdots, \rho_N, T_0\right]'. \tag{1}$$

We also define a pattern fidelity term

$$\Phi_{fidelity} = \sum_{i=1}^{N}\sum_{j=1}^{N}\frac{1}{2}\rho_i \boldsymbol{H}_{ij}\rho_j + \sum_{j=1}^{N} T_0 \boldsymbol{p}_j \rho_j + PT_0^2, \tag{2}$$

where

$$\boldsymbol{H}_{ij} = \frac{1}{2W^2}\sum_{n=1}^{P}\left[I^{(i)}\left(x_n^+\right) + I^{(i)}\left(x_n^-\right)\right]\left[I^{(j)}\left(x_n^+\right) + I^{(j)}\left(x_n^-\right)\right], \tag{3}$$

W is the total source intensity, and I is the intensity per incoherent pixel i at measurement point x. Pairs of measurement points are placed along the pattern edge, with x^+ just inside, and x^- just outside, for a total of $2P$ points, and

$$\boldsymbol{p}_j = -\frac{1}{W}\sum_{n=1}^{P}\left[I^{(j)}\left(x_n^+\right) + I^{(j)}\left(x_n^-\right)\right], \tag{4}$$

We now define an $\hat{\boldsymbol{H}}$ matrix, where

$$\hat{\boldsymbol{H}}_{ij} = \boldsymbol{H}_{ij}, i, j = 1, \cdots, N, \tag{5}$$

$$\hat{\boldsymbol{H}}_{N+1,j} = \hat{\boldsymbol{H}}_{j,N+1} = \boldsymbol{p}_j, \tag{6}$$

$$\hat{\boldsymbol{H}}_{N+1,N+1} = 2P. \tag{7}$$

Finally, the complete QP is stated as follows:

$$\min \frac{F}{2}\boldsymbol{q}'\hat{\boldsymbol{H}}\boldsymbol{q}+(1-F)\boldsymbol{c}'\boldsymbol{q}, \tag{8}$$

$$\text{s.t.}\sum_{i=1}^{N}\rho_i = W,$$

$$0 \le \rho_i \le 1,$$

$$T_0 \ge 0,$$

where F is a weight parameter, and $\boldsymbol{c}$ is a linear image log slope term, which will not be used in this investigation. Figure 1 shows two aerial images generated with optimized illuminators; we can see how the edge-placement error (EPE) term not only does its job reducing EPE, but also evens out the intensities within the pattern, reducing sharp peaks that lead to accelerated degradation of the mask and other components.

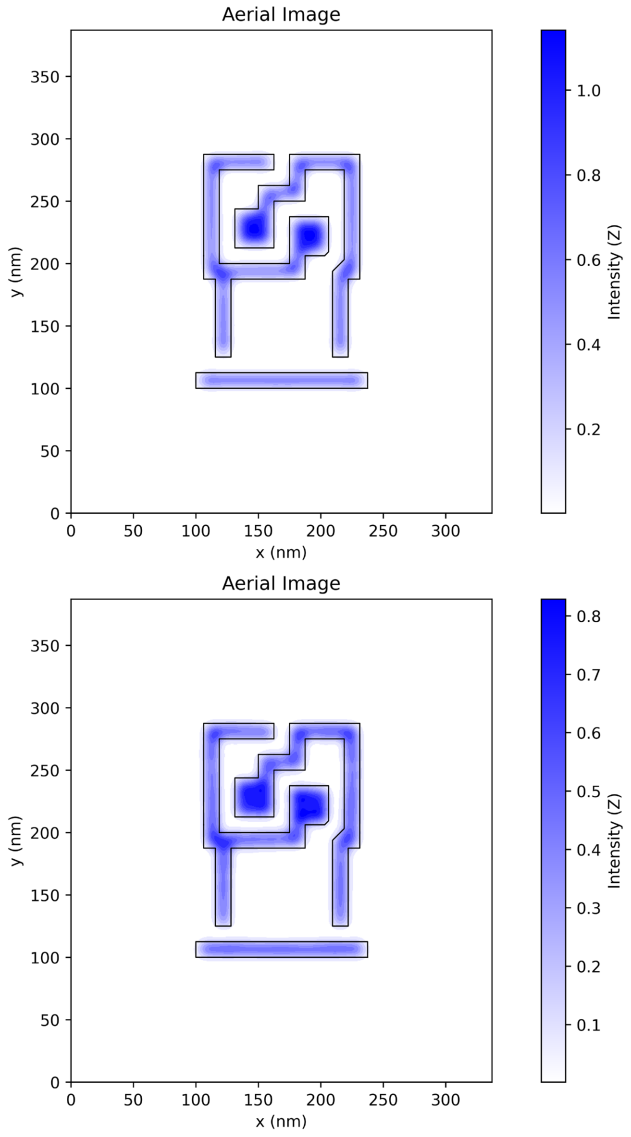

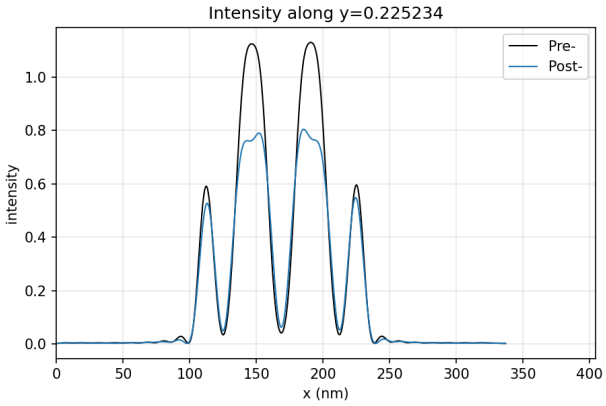
Intensity along y=0.225234
Pre-
Post-
intensity
x (nm)

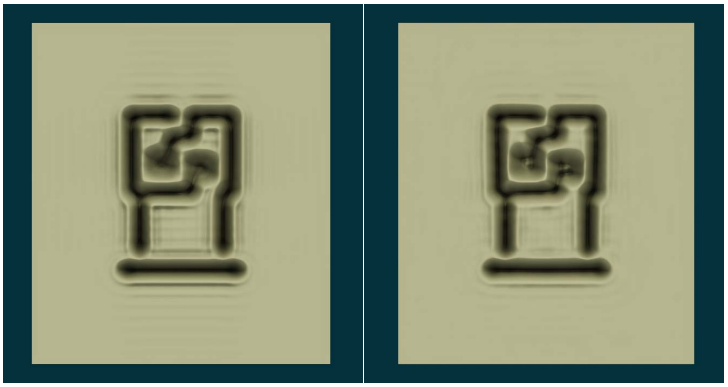

(a)

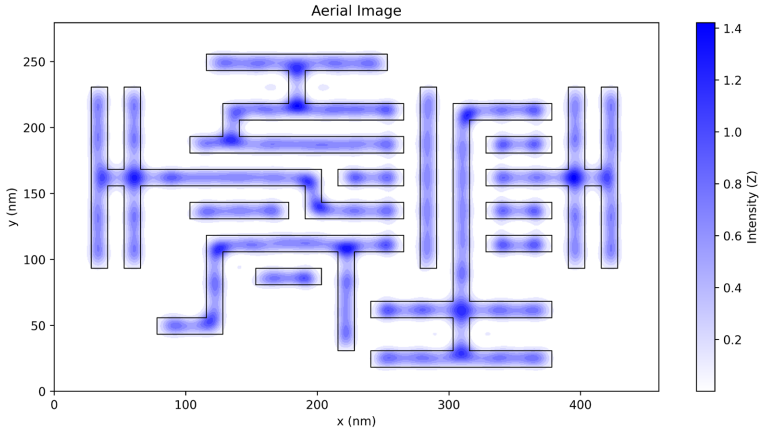
Aerial Image
y (nm)
x (nm)
Intensity (Z)

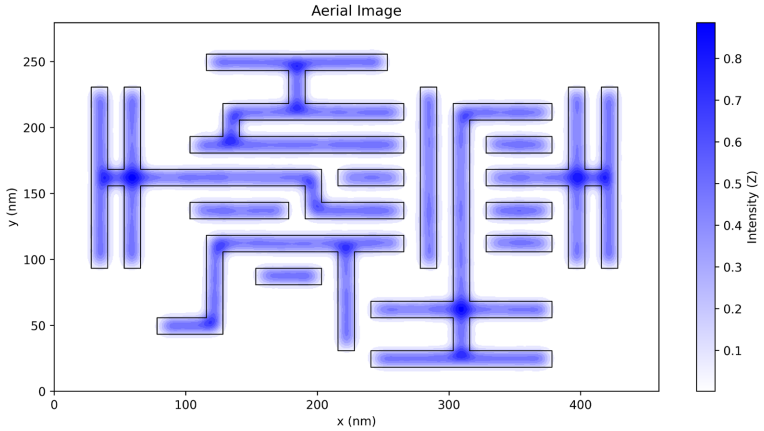
Aerial Image
y (nm)
x (nm)
Intensity (Z)

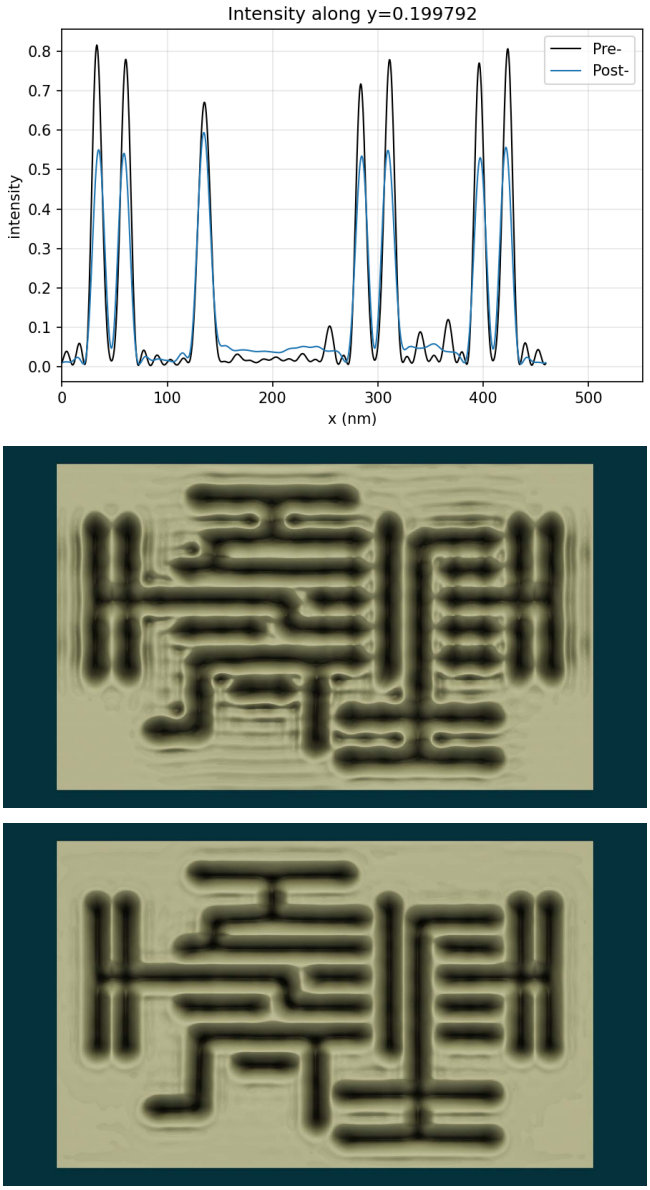

(b)

Figure 1. (a) Pre- and post-optimization of the small arbitrary pattern, showing the aerial image, intensity along $y = 225$, and a 3-dimensional surface plot. Circular illuminator, $W = 300$, $I_{\text{source,uniform}} = 0.1262$; (b) Pre- and post-optimization of the large arbitrary pattern, showing the aerial image, intensity along $y = 200$, and a 3-dimensional surface plot. Circular illuminator, $W = 300$, $I_{\text{source,uniform}} = 0.1262$.

To evaluate the presence of numerical instability in the solutions, we will first examine how the number of non-binary pixels varies as the optimization parameters are changed. Namely, we will vary the W parameter, the number of measurement points, and the number of features for a given pattern. Then, we will conduct a direct comparison between 64- and 128-bit precision on the following patterns: 4 symmetric contact holes, an asymmetric L shape, a small arbitrary pattern, and a large arbitrary pattern (**Figure 2**). The CD in all these patterns is 12.5

nm. These patterns were optimized for both a circular and annular illuminator (Figure 3). The combination of all these parameters equates to 8 different possible programs, which all were executed in 64- and 128-bit precision, for a total of 16 trials. We will define a pixel to be non-binary if $0.05 \le \rho_i \le 0.95$.

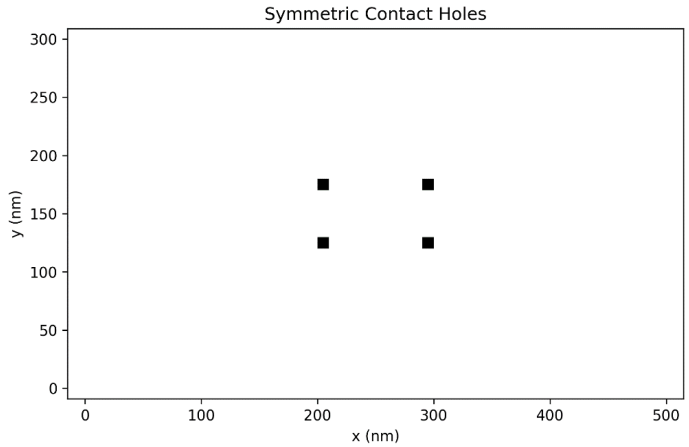

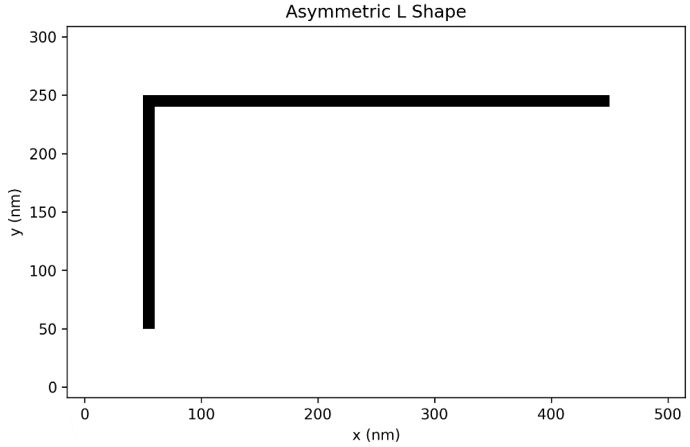

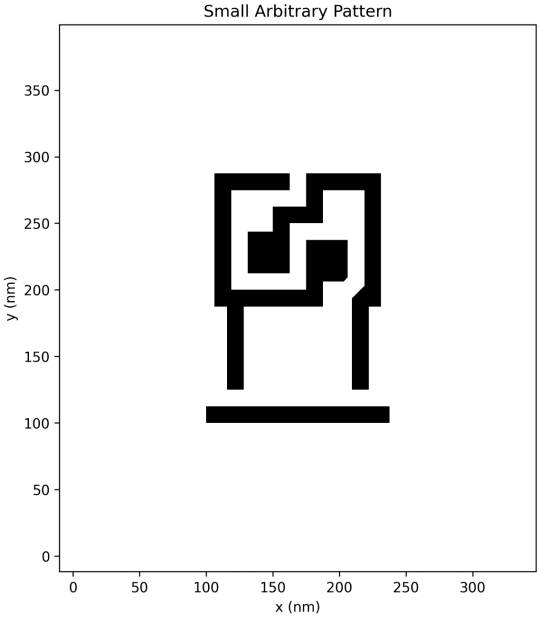

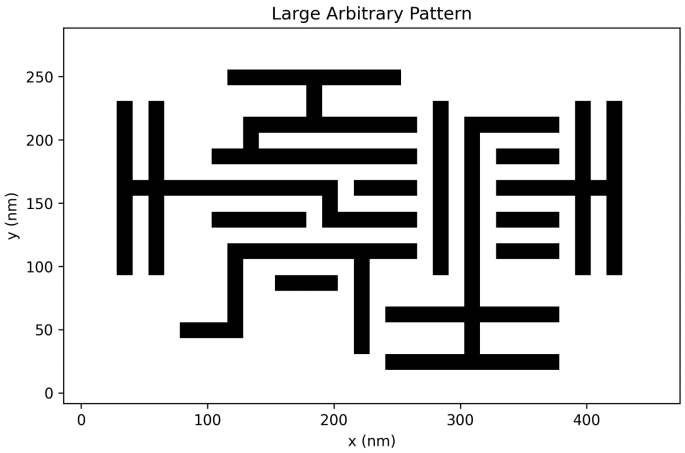

Figure 2. The 4 test patterns plotted.

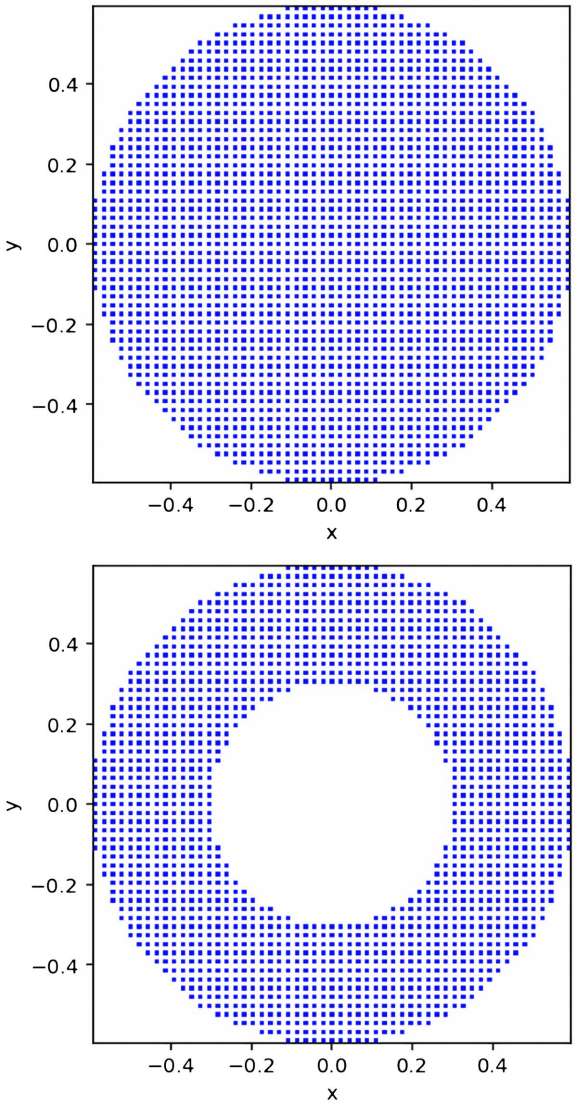

Figure 3. Circular and annular pixelated illuminators used; upper N_{pixel} = 2377, lower N_{pixel} = 1784.

As shown in the original paper's results, the quadratic term is responsible for the presence of non-binary pixels; setting $F = 0$ guarantees binary pixels, as the problem becomes a convex LP. Since our investigation is solely focused on non-binary pixels, the F parameter will be set to 1. Moreover, the W parameter will be set to 300, and all possible measurement points will be selected around the pattern, with the exclusion of the specific examination of each respective parameter.

For the lithography system, we assumed an EUV system with $\lambda = 13.5$ nm, NA = 0.55, a 4X uniform reduction factor, and a pixel resolution of 0.02 rad, leading to $N_{pixel} = 2377$ pixels inside the pupil. Additionally, we used a σ of 0.6, and an inner radius of 0.3 for the annular illuminator, for a total of $N_{pixel} = 1784$. We assumed a 2-dimensional, non-phase shifting mask.

To compute the aerial images, we used FAIM as the main simulation tool for our EUV system. The optimization program was written in C, largely based on the PETSc library [5]. We chose this path due to the easy switch between 64- and 128-bit precision, while also taking advantage of the TAO optimization library within PETSc. We used the primal-dual interior-point method (PDIPM) algorithm offered by TAO to perform the optimization. We also utilized some math routines from MPLAPACK since it supports a direct LU decomposition for a dense matrix, with multi-threaded calculations for both 64- and 128-bit precisions [6]. Python and MATLAB were used for data analysis.

Although PDIPM does not track an active set directly, whether the bound constraints are clearly identified at convergence still depends on strict complementarity between each primal variable and its bound multipliers. When the objective is ill-conditioned or rank-deficient, strict complementarity is no longer well-defined; the primal optimum is not unique on that face, and PDIPM converges to an interior point of the optimal face rather than to a vertex, leaving some coordinates at intermediate values. We refer to this condition as *active-set ambiguity*, and the experiments above are designed to test whether residual non-binary pixels are its numerical signature rather than a physical feature of the source optimization problem.

3. Results

For all trials, the optimization was left to run the maximum number of iterations until either no improvement to the solution gradient residual error, or an improvement of less than 5% to the solution gradient was achieved. In multiple trials, cyclical behavior was observed at the optimal point with no numerical change to the cost function down to 32 digits (in the 128-bit case). In most cases, this behavior occurred for either exactly 1 or 2 iterations. As such, we configured the optimization to stop at 3 consecutive iterations where the above condition was met. This led to a minimum of $\sim 10^{-15}$ residual error for 64-bit runs, and $\sim 10^{-32}$ residual error for 128-bit runs.

We will now discuss the effect of the different problem parameters on the number of non-binary pixels. Starting with the total source power W (**Figure 4**), we

can see an obvious downward trend as $W \to N_{pixels}$ eventually reaching 0. This is to be expected, as increasing W tightens the equality constraint of the convex set, forcing interior solution to the boundary. As such, lower W values allow for more degrees of freedom. However, between $W = 500$ and $W = 1500$, we see that there is a large variation in the number of non-binary pixels, ranging from 28 to 7, with large jumps noticed between sequential optimizations.

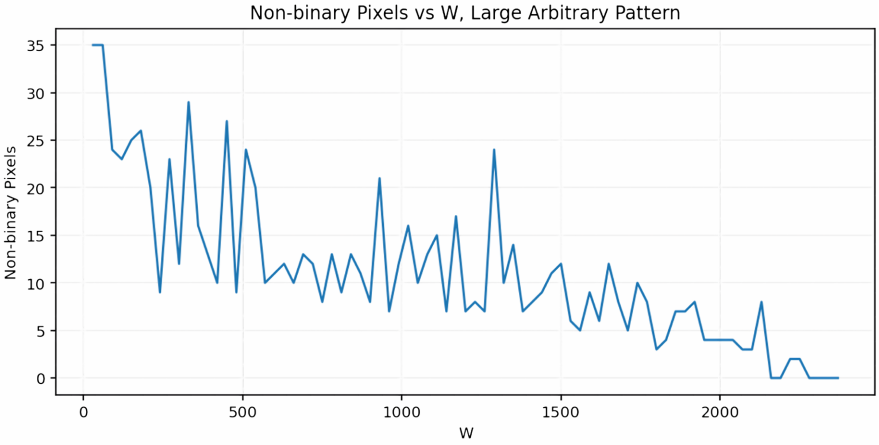

Figure 4. Change in non-binary pixels as source power varies; $\Delta W = 12$, large arbitrary pattern, circular illuminator.

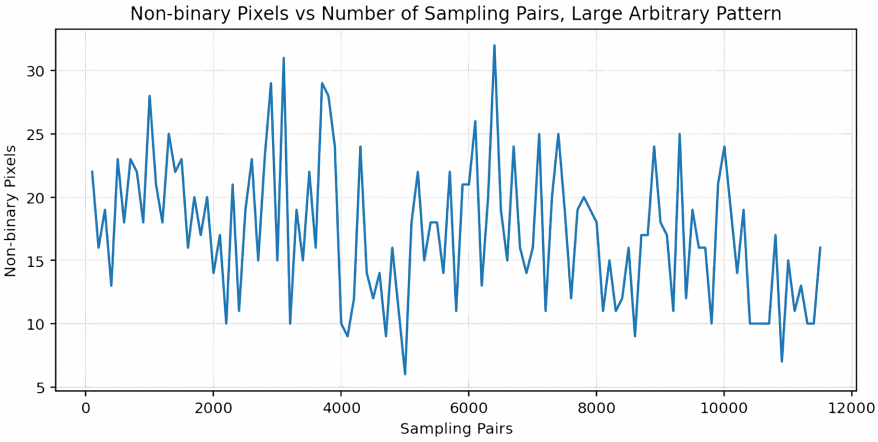

Figure 5. Change in non-binary pixels as the number of measurement pairs varies (equally spaced); $\Delta P = 100$, large arbitrary pattern, circular illuminator.

Figure 5 shows the effect of varying the number of evenly spaced measurement pairs across the edge of the pattern. Namely, varying this parameter produced non-monotonic changes in the number of non-binary pixels, with noticeable sequential jumps. Looking at the formulation of the QP, and any aerial image, we can see that intensities vary significantly across the edge of a pattern, specifically close to junctions or corners. As such, the variation of the solution is to be expected with a non-negligible change to the cost function. Moreover, in Figure 6 we show the effect of the same number ($p = 100$) but differently placed measure-

ment pairs across the pattern; namely, the selection of pairs vastly changes the shape of the optimized source, which results in measurable changes to the aerial image and NILS. However: if we randomize the location of all points while keeping the number the same, the optimized source will contain the same number of non-binary points. This decoupling is a key observation: the two runs correspond to genuinely different optimization problems and yield different illuminators (Figure 6), yet the residual non-binary count is identical. If these pixels encoded something physical about the imaging problem, their number should track the changes in the fidelity objective and the resulting aerial image. The fact that it does not, while every other feature of the solution does, indicates that the residual count is not set by the lithography process and is consistent with a numerical origin. In addition, we show in Figure 7 that the non-binary intensities do not contribute to the aerial image in a measurable manner. By rounding-off intensities to the nearest integer, we can see that the mean and variation in EPE and NILS across the aerial image are effectively unchanged. These observations point to the presence of some sort of numerical instability.

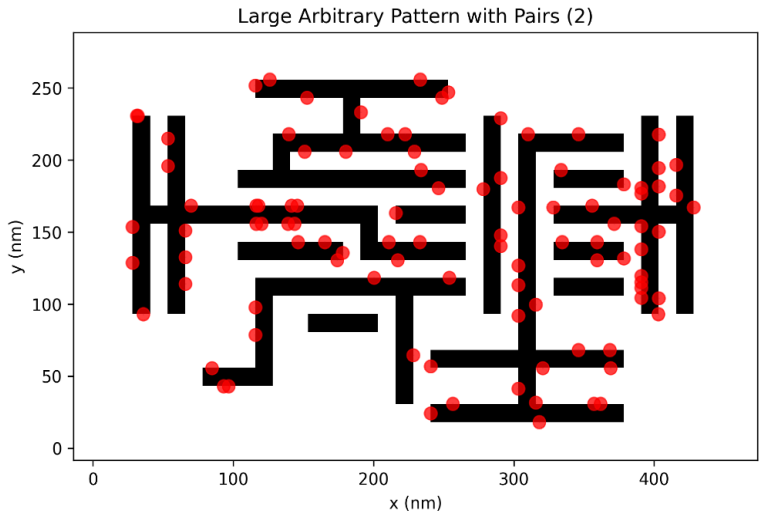

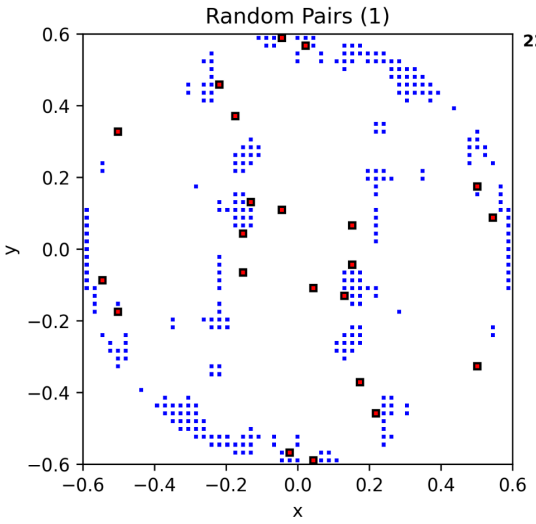

22 Non-binary pixels

x	y	val
0.153	0.0655	0.1591
0.545	0.0873	0.785
0.502	0.175	0.2755
0.0218	0.567	0.1835
-0.153	0.0436	0.4635
-0.0436	0.109	0.6282
-0.131	0.131	0.5191
-0.502	0.327	0.8858
-0.175	0.371	0.7422
-0.218	0.458	0.5469
-0.0436	0.589	0.6959
-0.0218	-0.567	0.835
-0.502	-0.175	0.06455
-0.545	-0.0873	0.6099
-0.153	-0.0655	0.1474
0.0436	-0.589	0.05517
0.218	-0.458	0.7469
0.175	-0.371	0.2231
0.502	-0.327	0.2164
0.131	-0.131	0.05644
0.0436	-0.109	0.4236
0.153	-0.0436	0.71

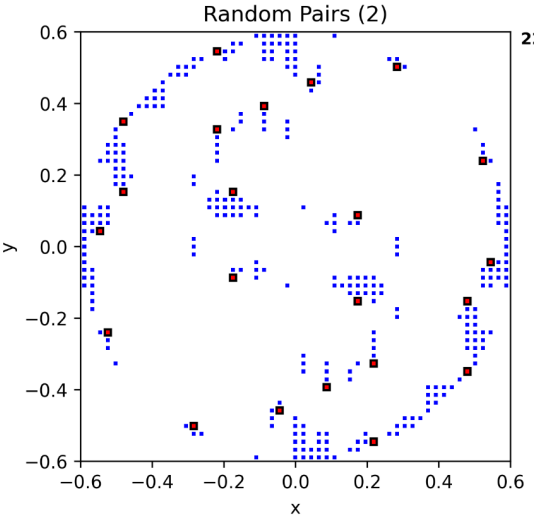

22 Non-binary pixels

x	y	val
0.175	0.0873	0.7988
0.524	0.24	0.1526
0.0436	0.458	0.1249
0.284	0.502	0.0523
-0.545	0.0436	0.9035
-0.48	0.153	0.4892
-0.175	0.153	0.06171
-0.218	0.327	0.07071
-0.48	0.349	0.897
-0.0873	0.393	0.6742
-0.218	0.545	0.1598
-0.284	-0.502	0.05244
-0.0436	-0.458	0.165
-0.524	-0.24	0.1979
-0.175	-0.0873	0.7351
0.218	-0.545	0.2161
0.0873	-0.393	0.3182
0.48	-0.349	0.3989
0.218	-0.327	0.0822
0.175	-0.153	0.07514
0.48	-0.153	0.6831
0.545	-0.0436	0.769

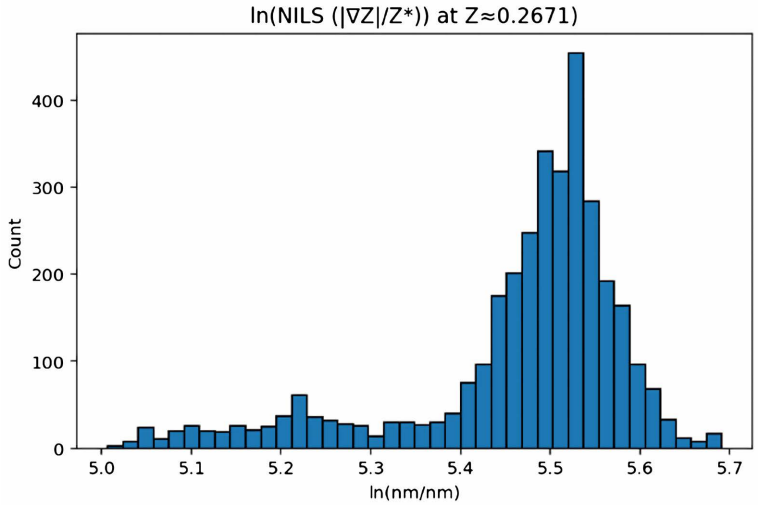

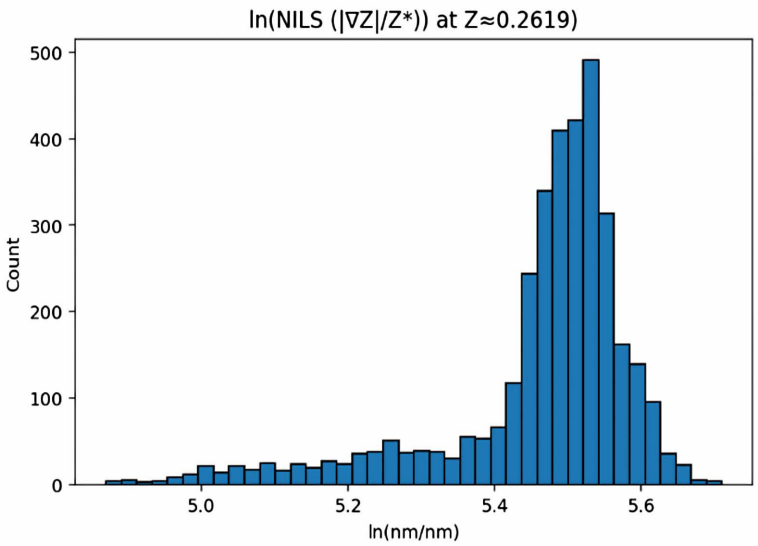

Figure 6. Effect of optimized source solution of random placement of $p = 100$ points. The number of non-binary points was $n = 22$ in both simulations.

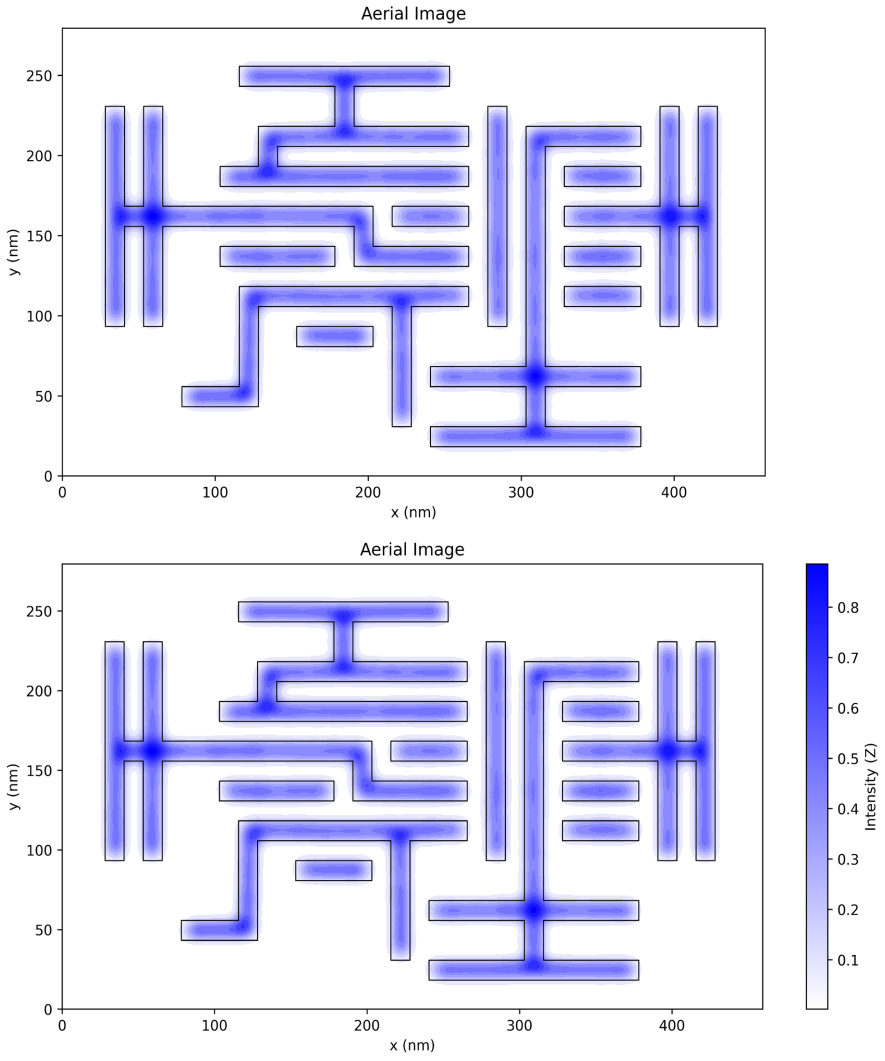

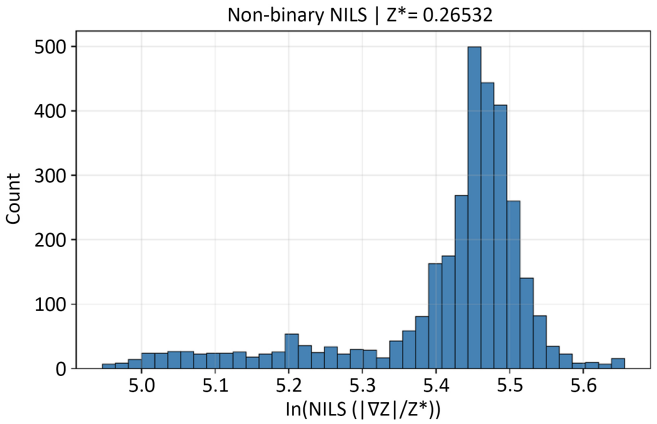

NILS statistics

N selected	3269
Variance	0.01629
Std Dev	0.1276
Mean	5.414
Min	4.947
Max	5.656

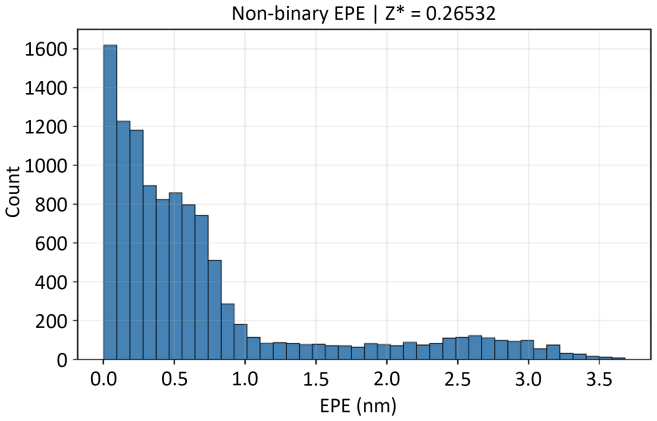

EPE statistics (nm)

N contour pts	11298
Mean	0.7242
Variance	0.6598
Std Dev	0.8123
Min	0.002368
Max	3.68

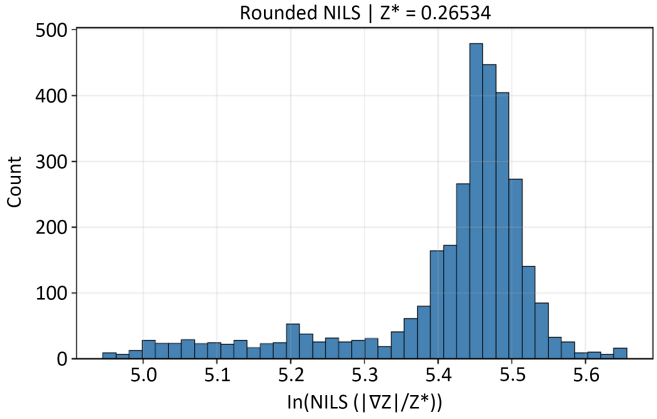

NILS statistics

N selected	3266
Variance	0.01654
Std Dev	0.1286
Mean	5.413
Min	4.945
Max	5.656

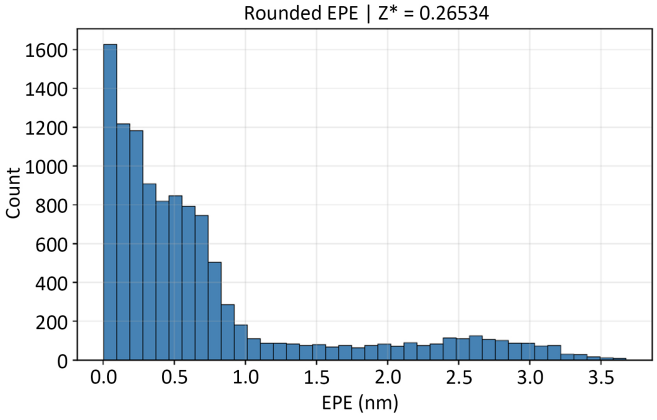

EPE statistics (nm)

N contour pts	11296
Mean	0.7237
Variance	0.6598
Std Dev	0.8123
Min	0.002492
Max	3.676

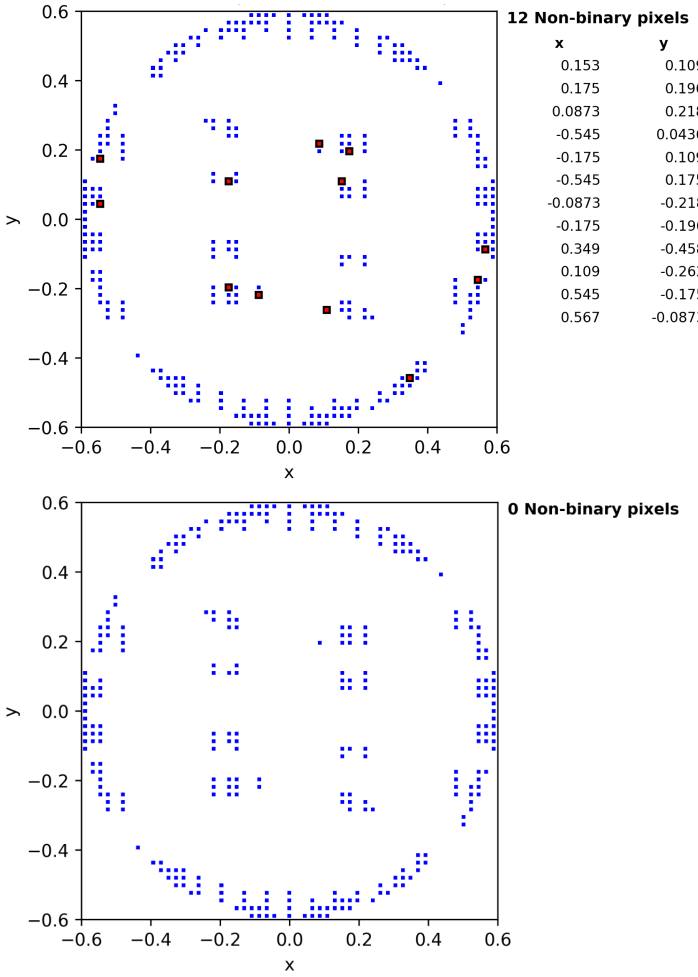

Figure 7. Upper: optimal solution to the large arbitrary pattern with a circular illuminator. Lower: rounded non-binary intensities. The variation of the aerial image, average EPE, and NILS are insignificant.

Finally, we compared the effect of higher numerical precision on the optimization algorithm. After the intensities were calculated with 64-bit precision, the optimizer was run in both 64- and 128-bit precision for all 8 cases. **Figures 8-15** definitively show that higher numerical precision consistently yields fewer non-binary pixels in the optimized source. This behavior is consistent with numerical sensitivity of constrained QP optimization. Looking deeper into the formulation, the fidelity objective constructed from infinitely close measurement points can lead to near singular matrices, and consequently to near degeneracy in the KKT system. This fact is further confirmed by the insignificant contribution of these non-binary points, as discussed earlier. Increasing arithmetic precision to 128 bits decreases roundoff error during assembly of H and p, decreasing the effect of near cancelling terms.

This effect is further confirmed when comparing solutions of the same pattern with a circular and annular illuminator, specifically where the pixels removed were not present in the circular source. Looking at **Figure 8** and **Figure 9**, we can

see that although the optimized source has the same shape and no pixels were removed from the solution, the number of non-binary pixels is different (decreased from 3 to 0 in the 64-bit case). If the problem had a unique optimum with a stable active set, then removing pixels that are exactly zero at the optimum would not change the optimal solution on the remaining coordinates. The fact that the reduced problem yields an almost identical pattern, but a slightly different number of non-binary pixels indicates the solution is not strictly unique/not strongly stable: there are weakly determined degrees of freedom, and the active set is sensitive.

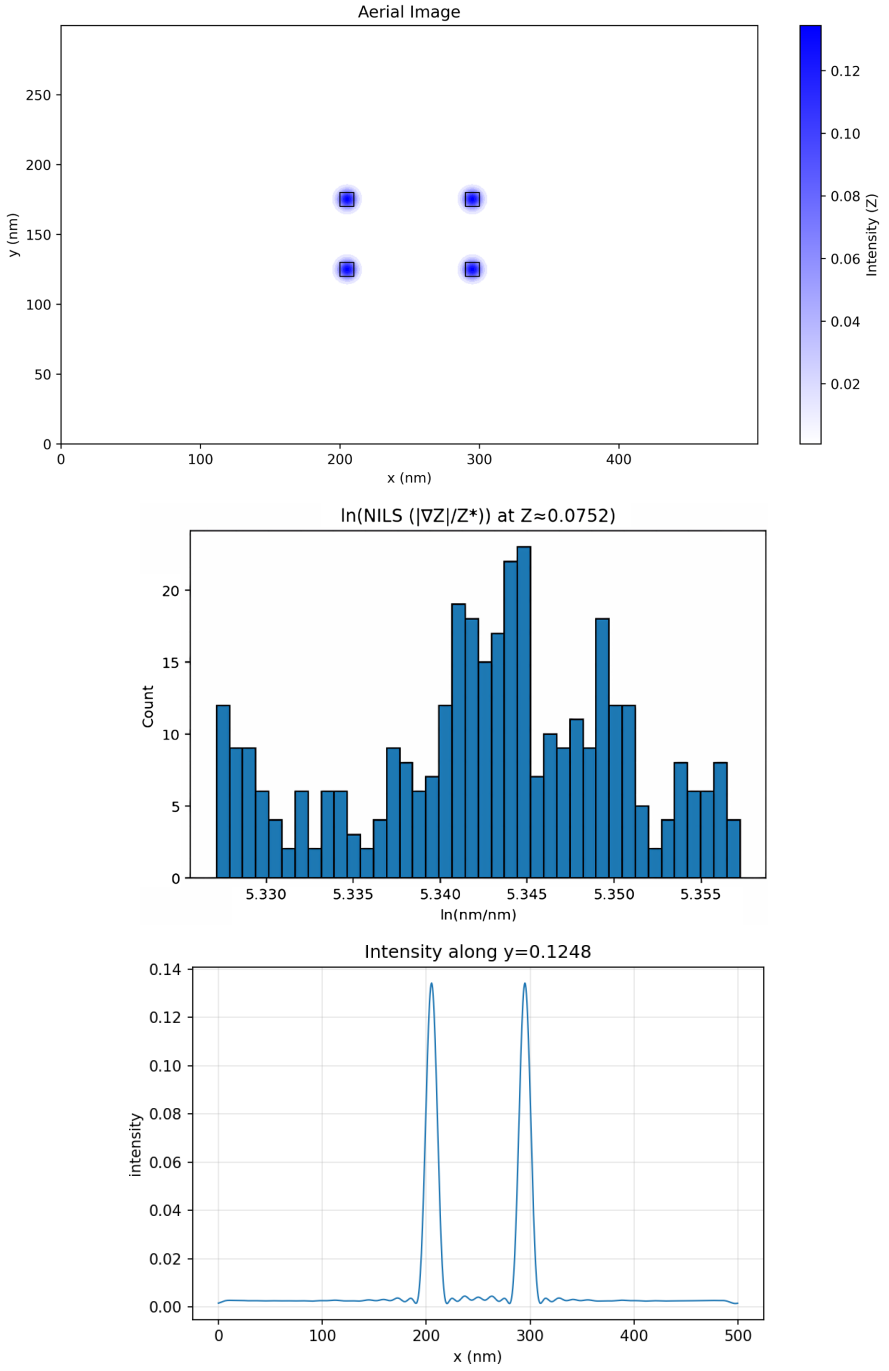

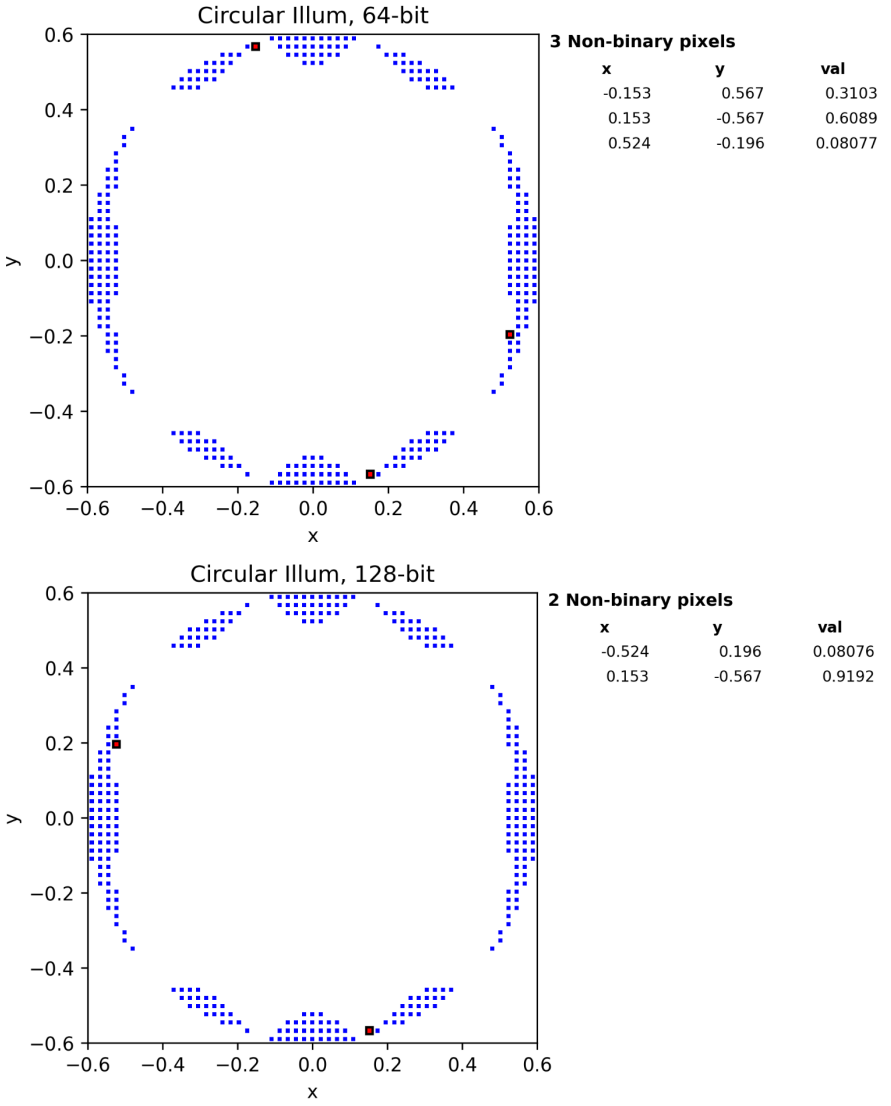

Figure 8. Symmetric contact holes/circular illuminator; aerial image, NILS histogram, line intensity, and illuminator plots in 64- and 128-bit precision.

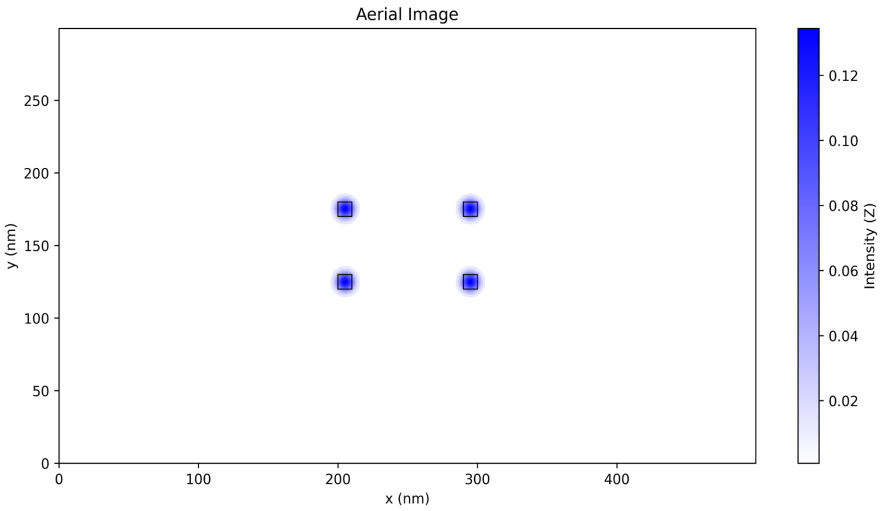

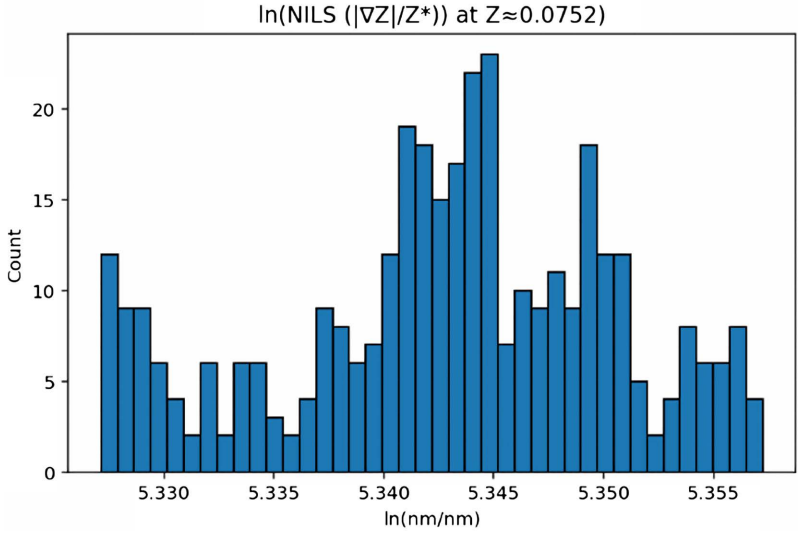
ln(NILS (|∇Z|/Z*)) at Z≈0.0752)
Count
ln(nm/nm)

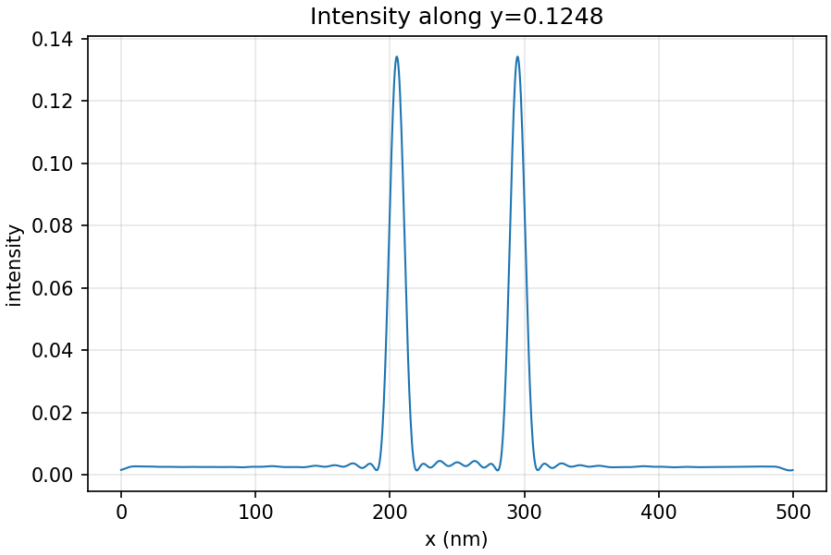
Intensity along y=0.1248
intensity
x (nm)

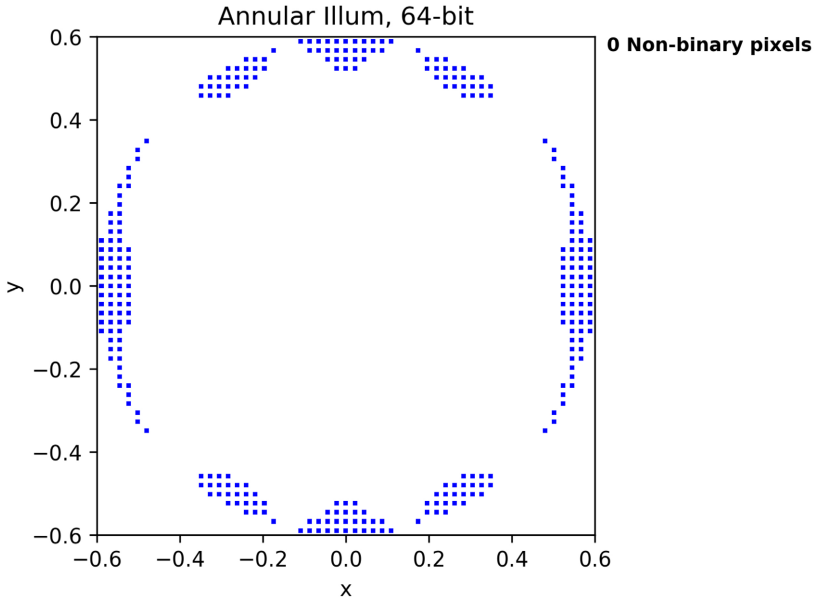
Annular Illum, 64-bit
0 Non-binary pixels
y
x

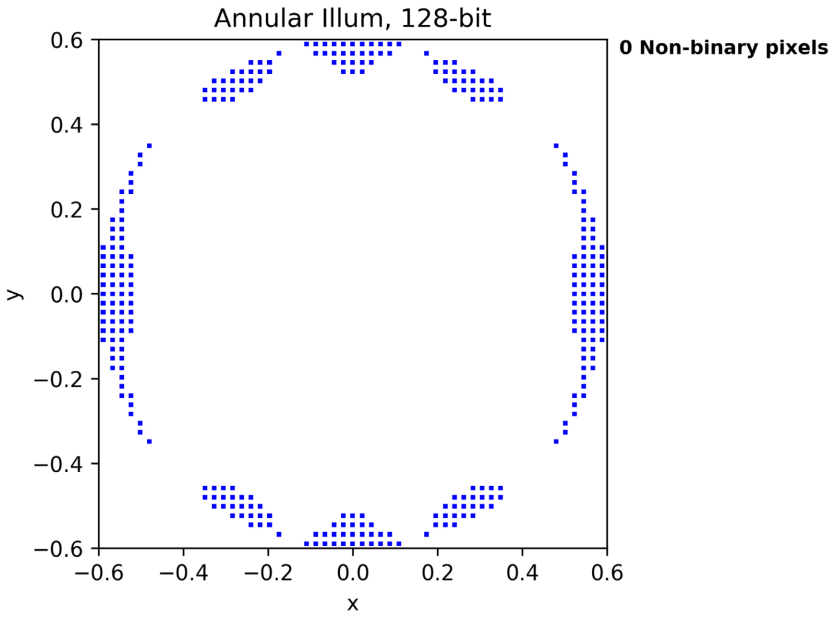

Figure 9. Symmetric contact holes/annular illuminator; aerial image, NILS histogram, line intensity, and illuminator plots in 64- and 128-bit precision.

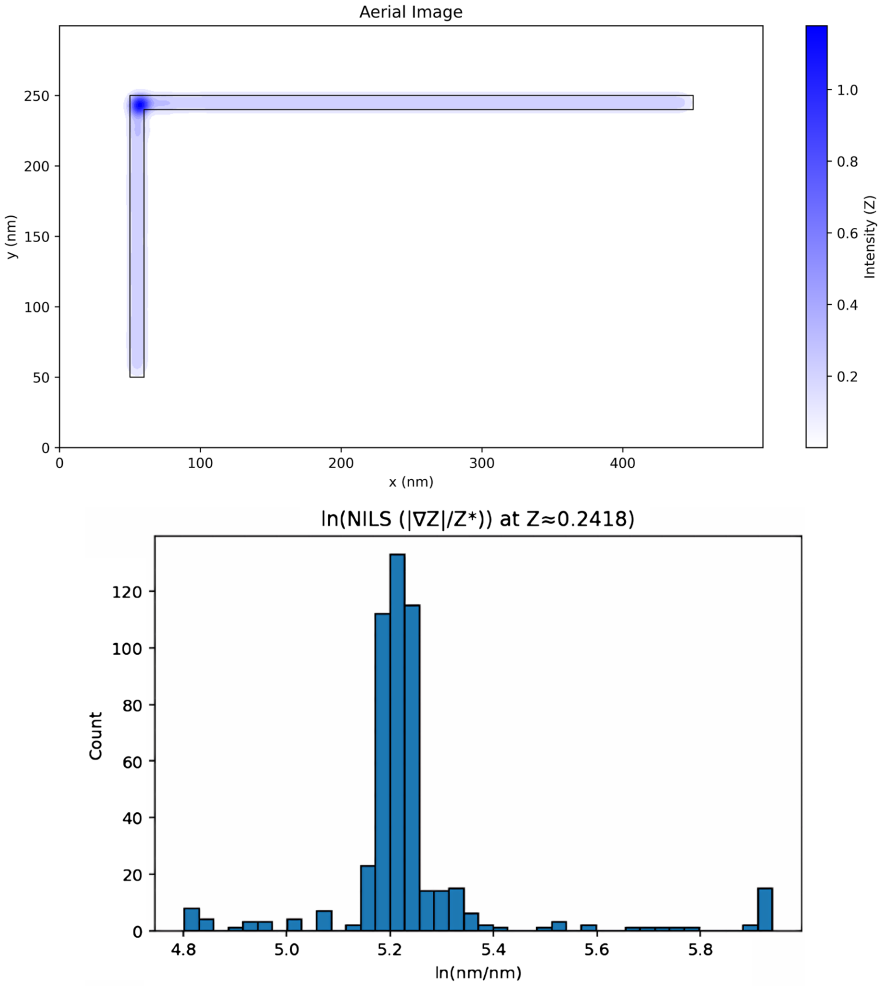

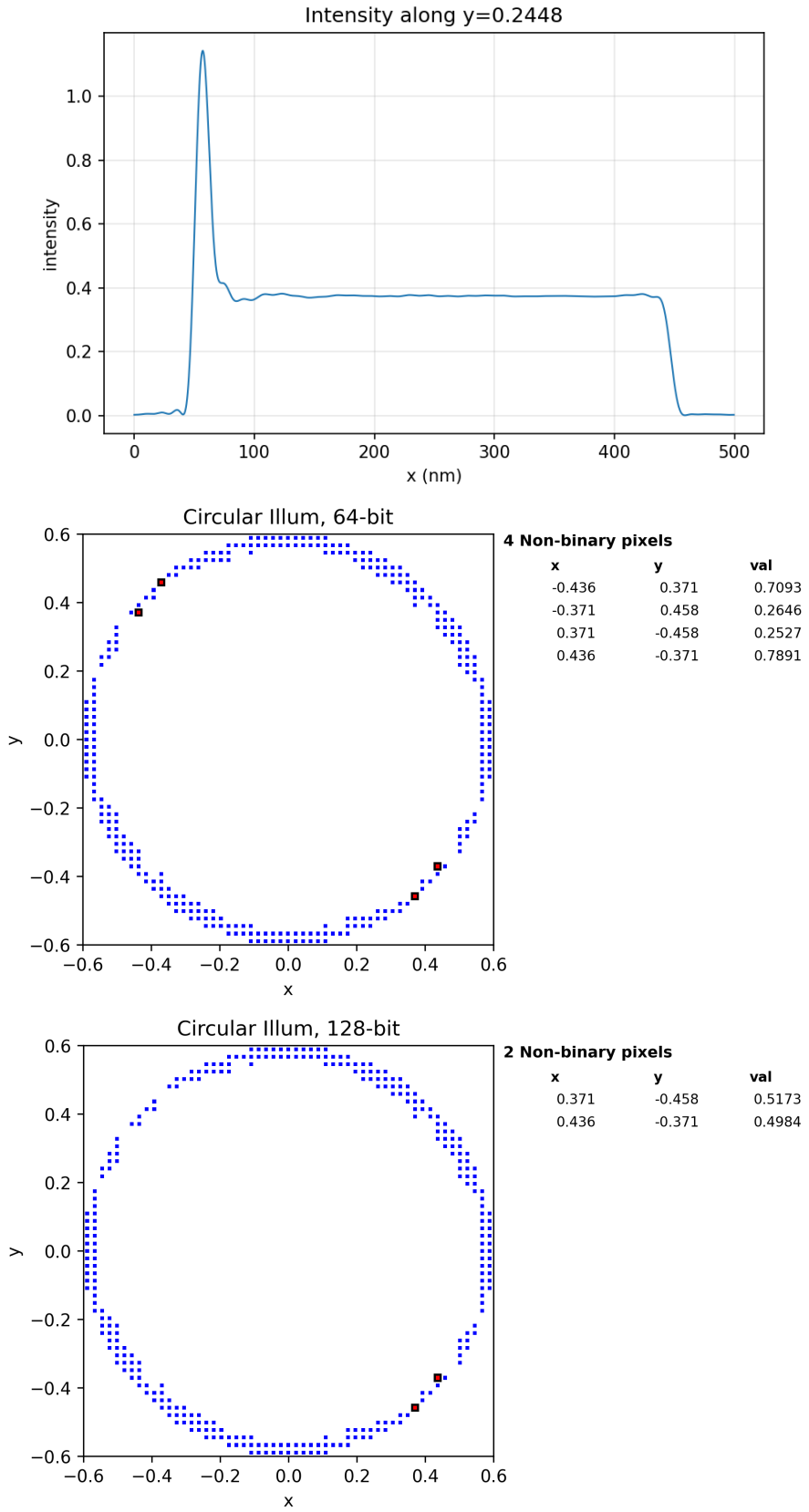

Figure 10. Asymmetric L shape/circular illuminator; aerial image, NILS histogram, line intensity, and illuminator plots in 64- and 128-bit precision.

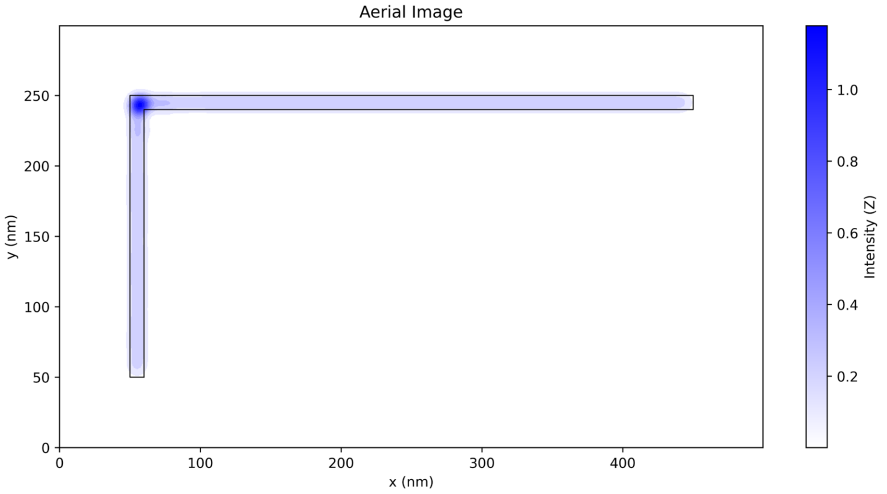
Aerial Image
y (nm)
x (nm)
Intensity (Z)

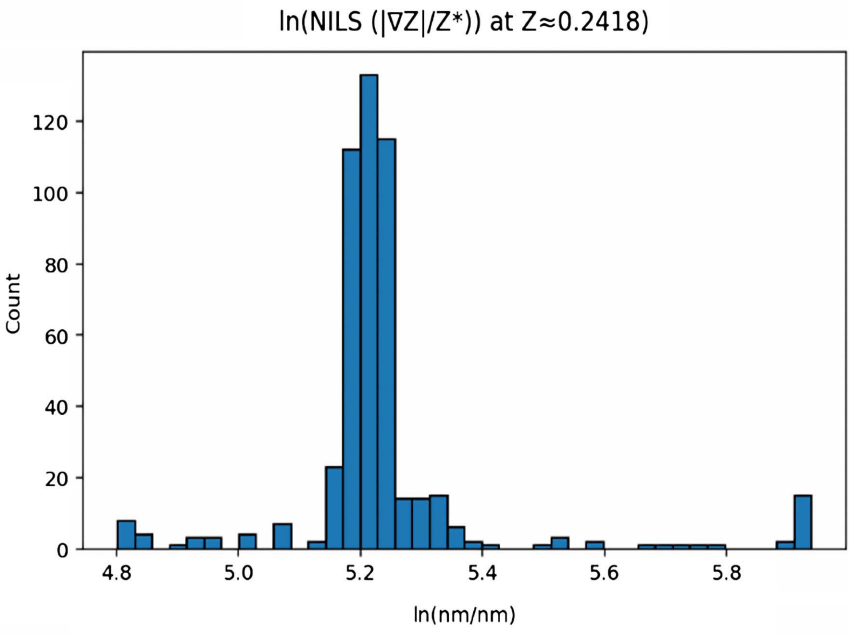
ln(NILS (|∇Z|/Z*)) at Z≈0.2418)
Count
ln(nm/nm)

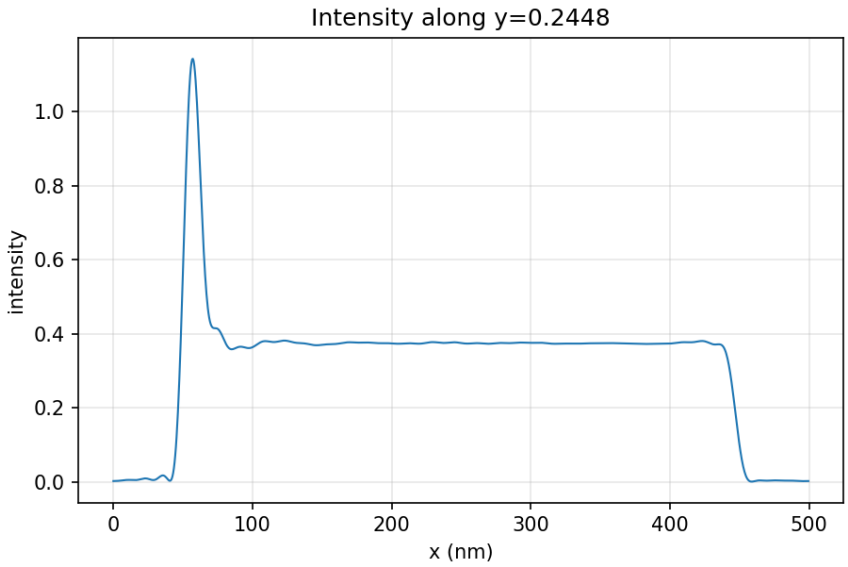
Intensity along y=0.2448
intensity
x (nm)

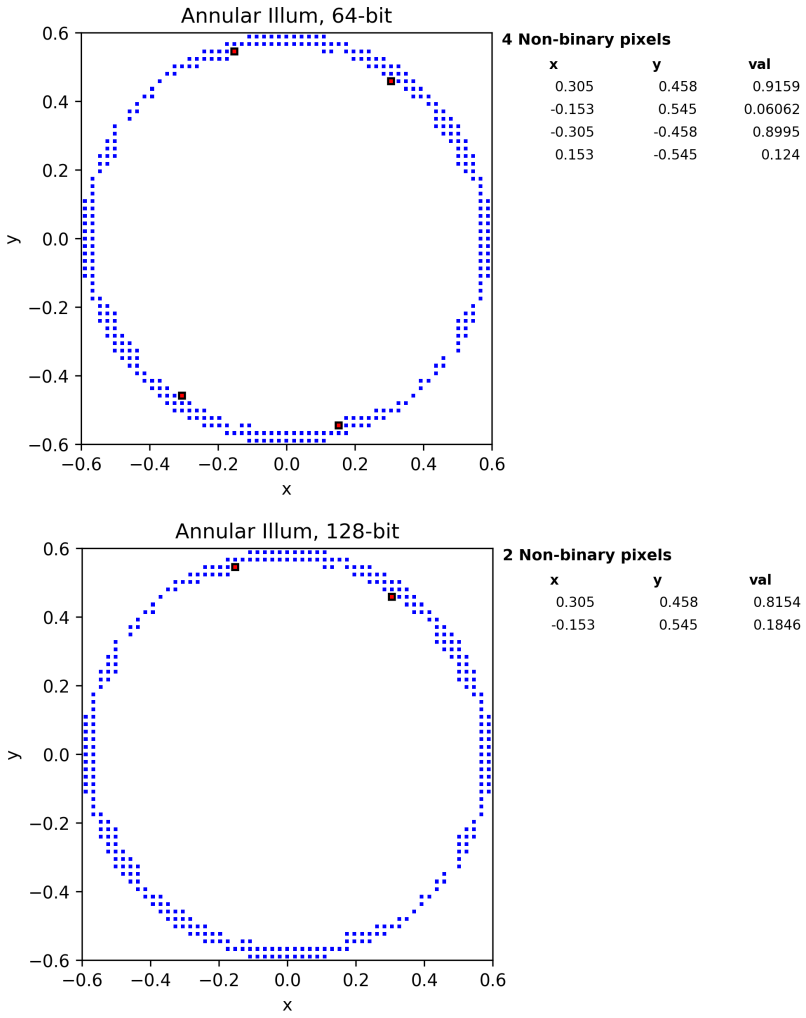

Figure 11. Asymmetric L shape/annular illuminator; aerial image, NILS histogram, line intensity, and illuminator plots in 64- and 128-bit precision.

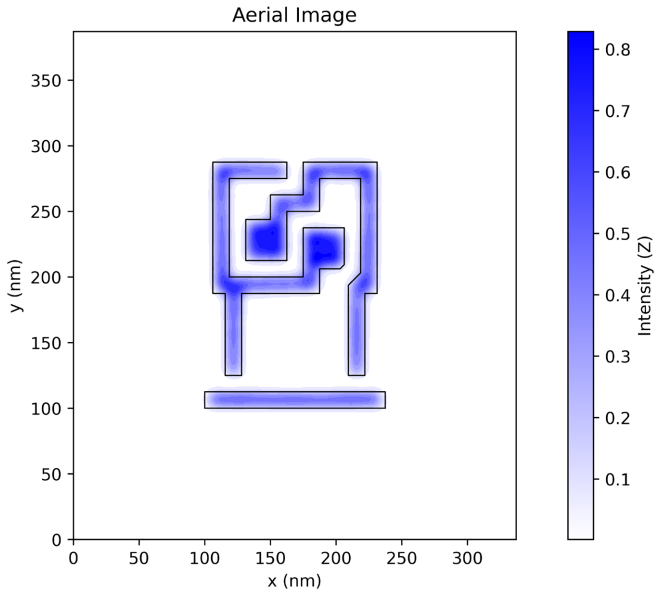

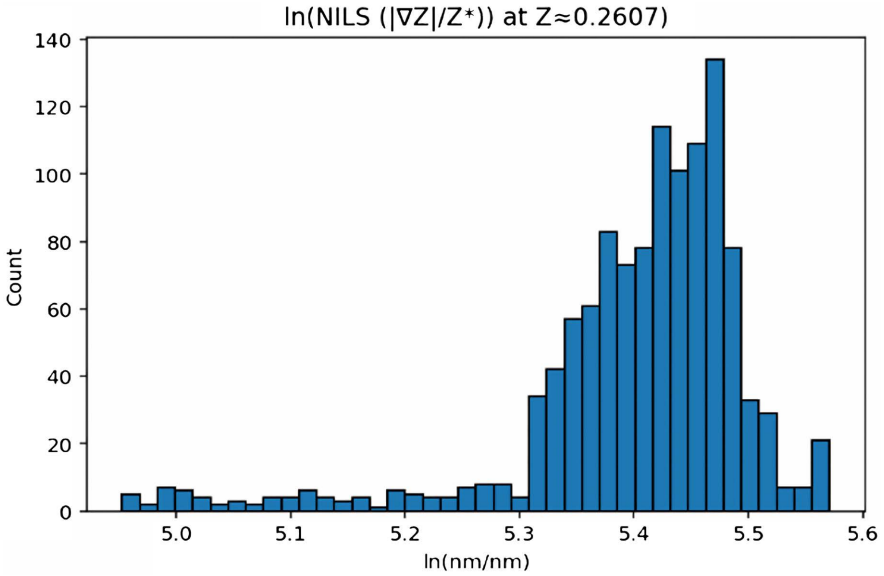

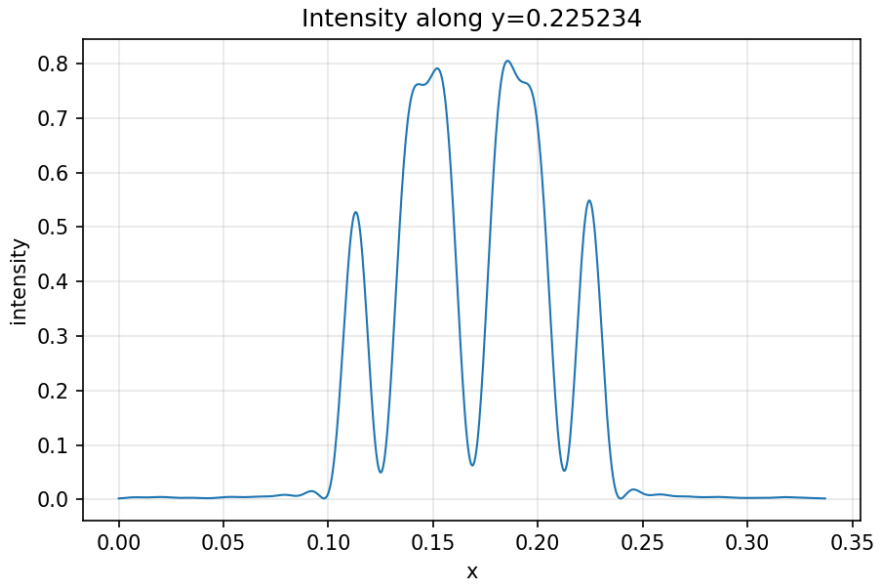

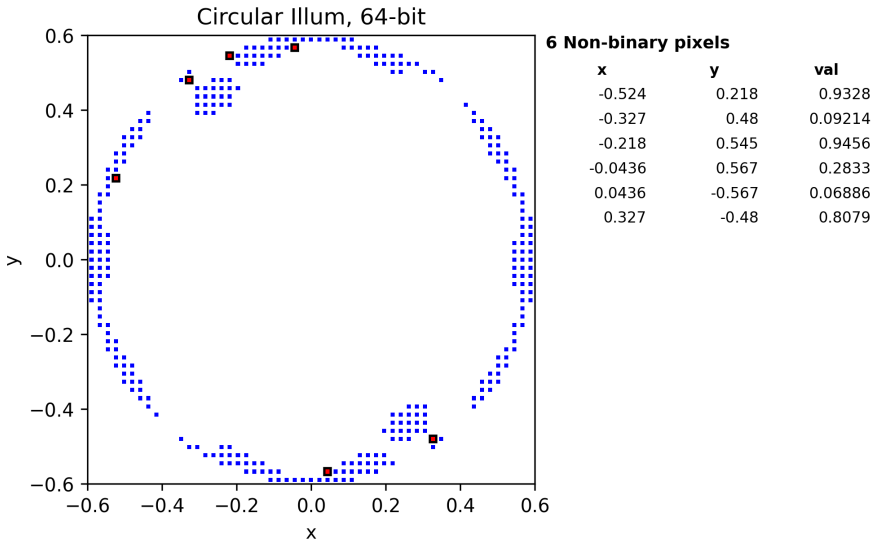

6 Non-binary pixels

x	y	val
-0.524	0.218	0.9328
-0.327	0.48	0.09214
-0.218	0.545	0.9456
-0.0436	0.567	0.2833
0.0436	-0.567	0.06886
0.327	-0.48	0.8079

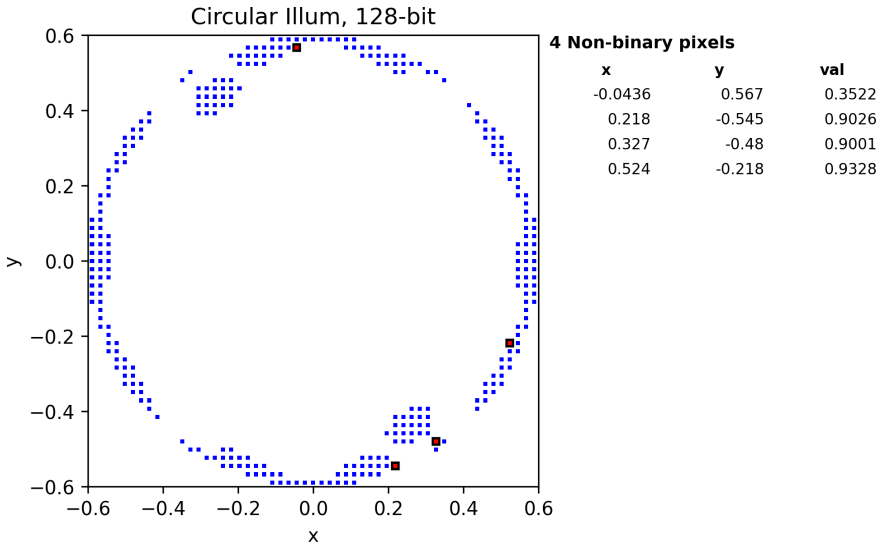

Figure 12. Small arbitrary pattern/circular illuminator; aerial image, NILS histogram, line intensity, and illuminator plots in 64- and 128-bit precision.

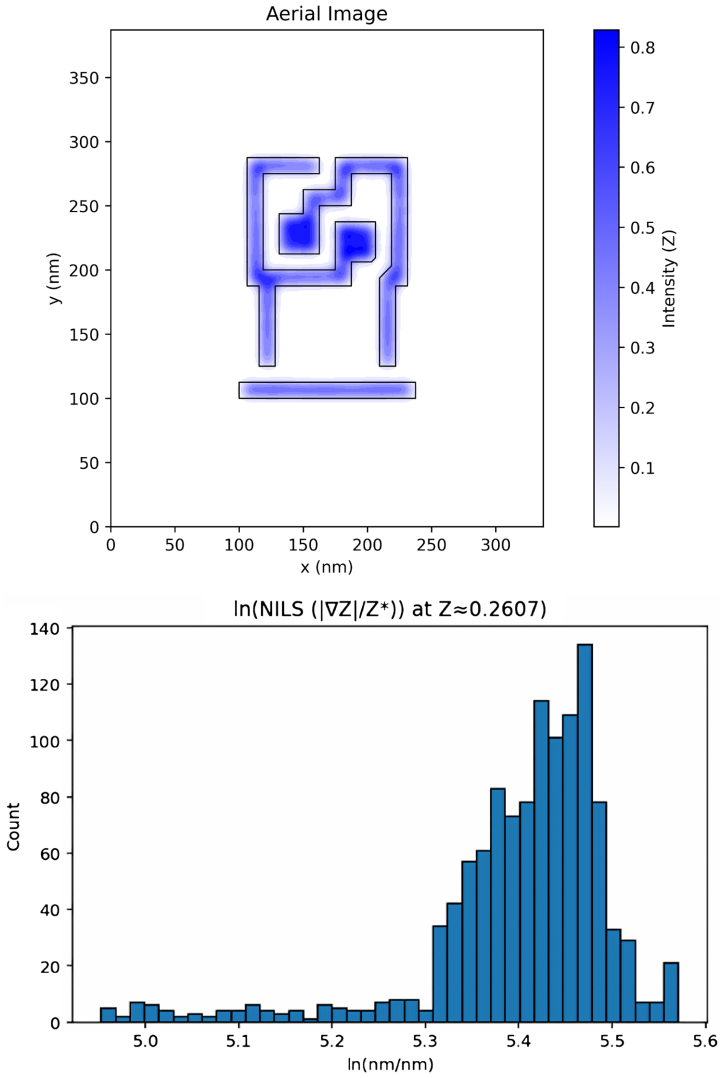

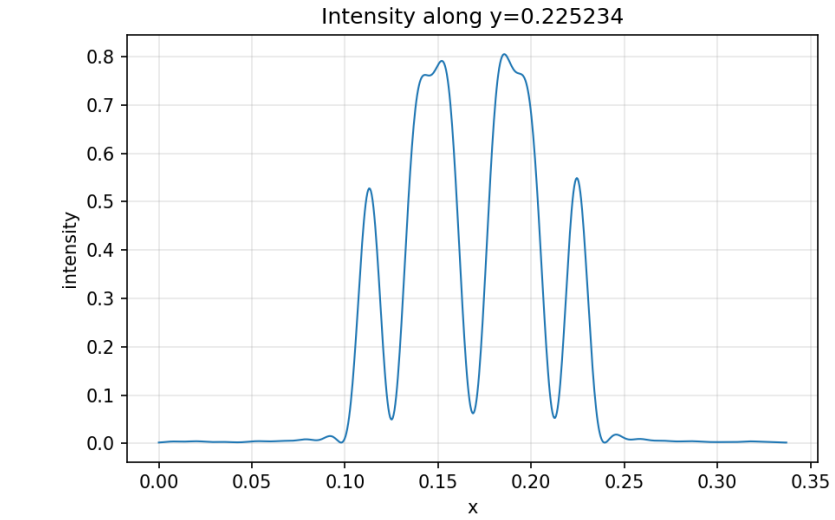

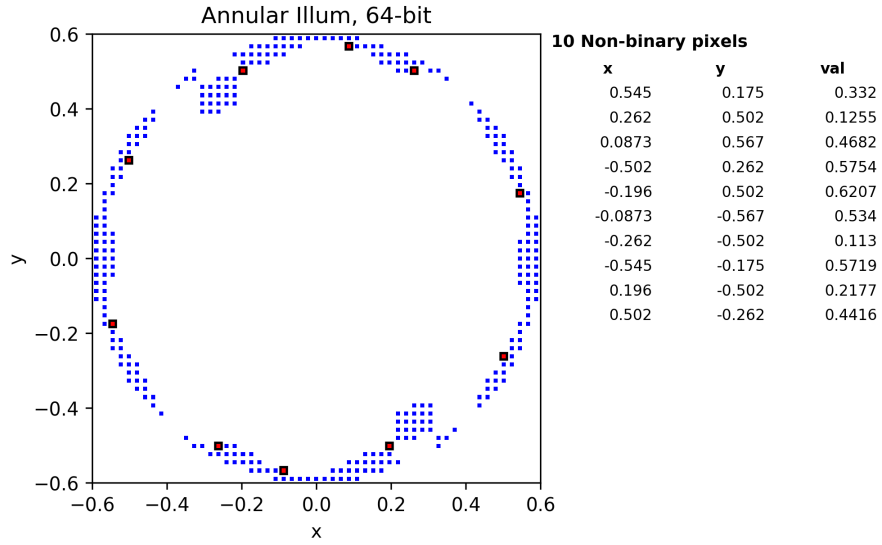

10 Non-binary pixels

x	y	val
0.545	0.175	0.332
0.262	0.502	0.1255
0.0873	0.567	0.4682
-0.502	0.262	0.5754
-0.196	0.502	0.6207
-0.0873	-0.567	0.534
-0.262	-0.502	0.113
-0.545	-0.175	0.5719
0.196	-0.502	0.2177
0.502	-0.262	0.4416

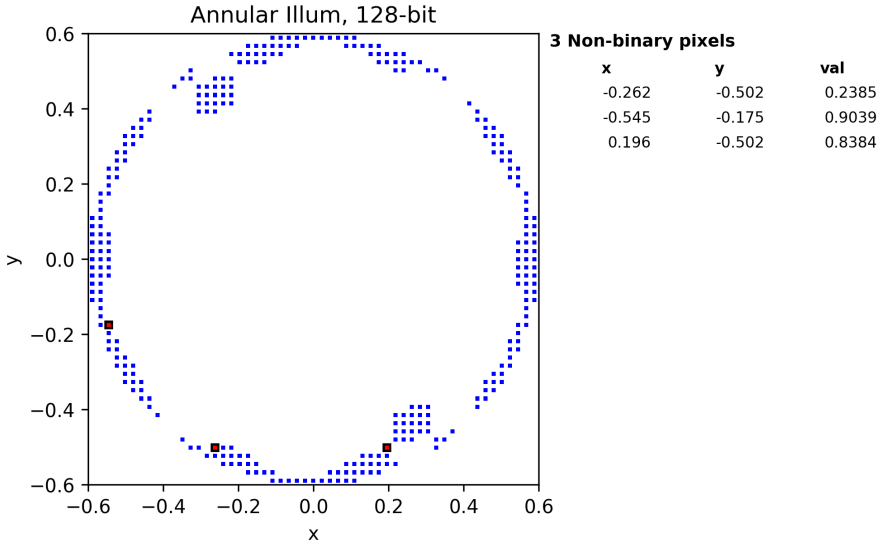

3 Non-binary pixels

x	y	val
-0.262	-0.502	0.2385
-0.545	-0.175	0.9039
0.196	-0.502	0.8384

Figure 13. Small arbitrary pattern/circular illuminator aerial image, NILS histogram, line intensity, and illuminator plots in 64- and 128-bit precision.

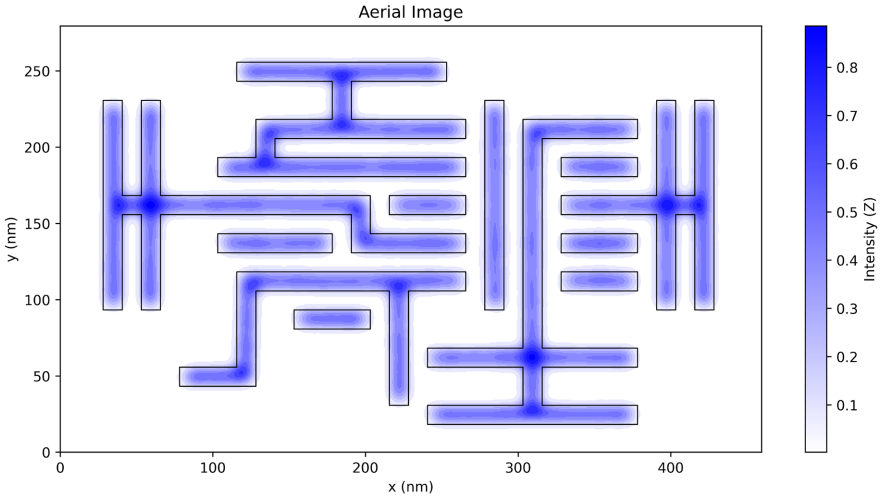
Aerial Image
y (nm)
x (nm)
Intensity (Z)

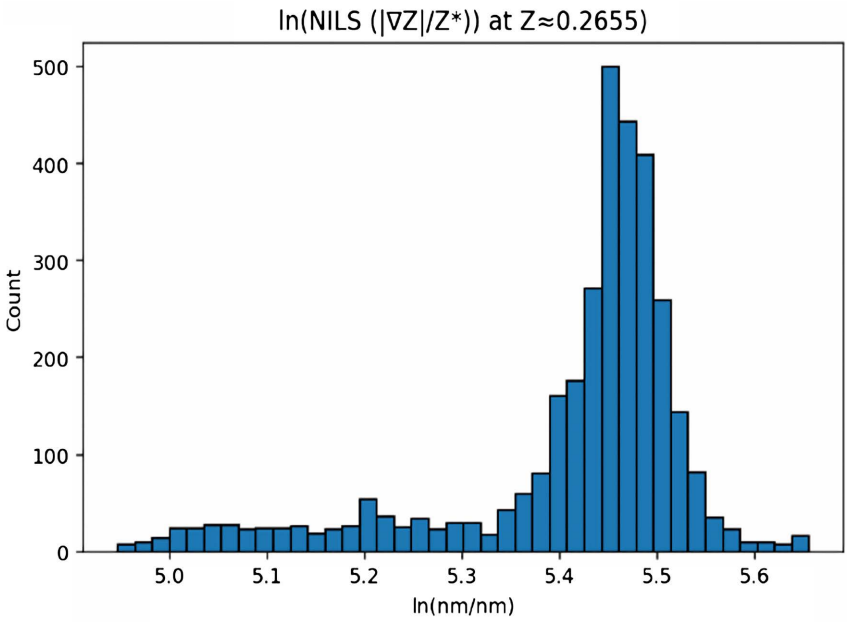
ln(NILS (|∇Z|/Z*)) at Z≈0.2655)
Count
ln(nm/nm)

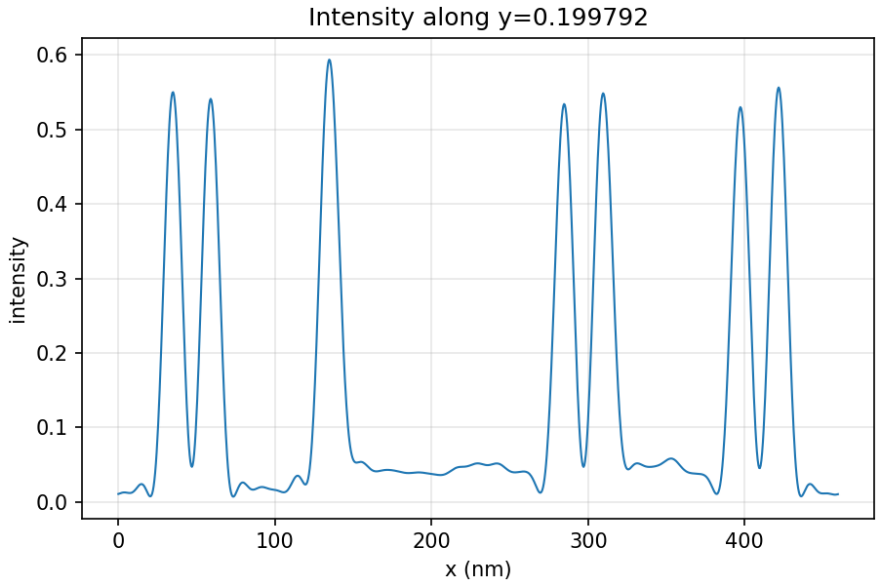
Intensity along y=0.199792
intensity
x (nm)

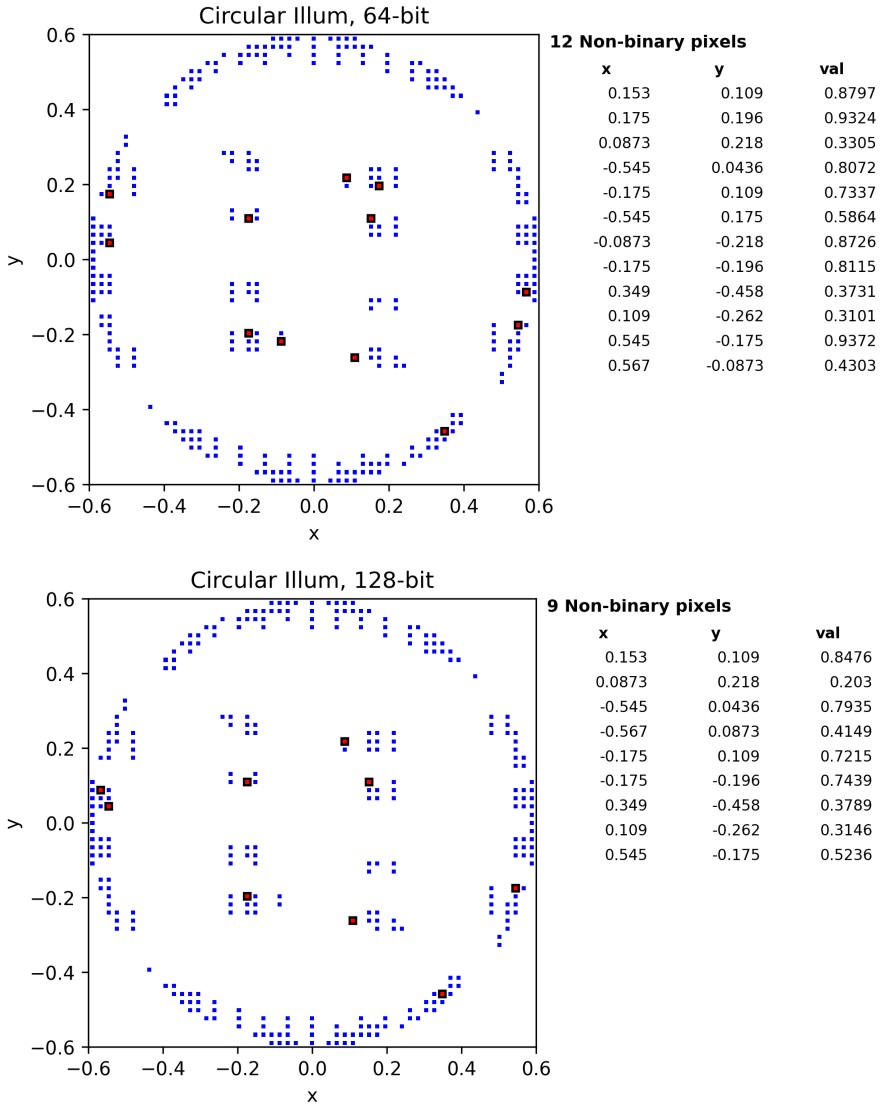

Figure 14. Large arbitrary pattern/circular illuminator; aerial image, NILS histogram, line intensity, and illuminator plots in 64- and 128-bit precision.

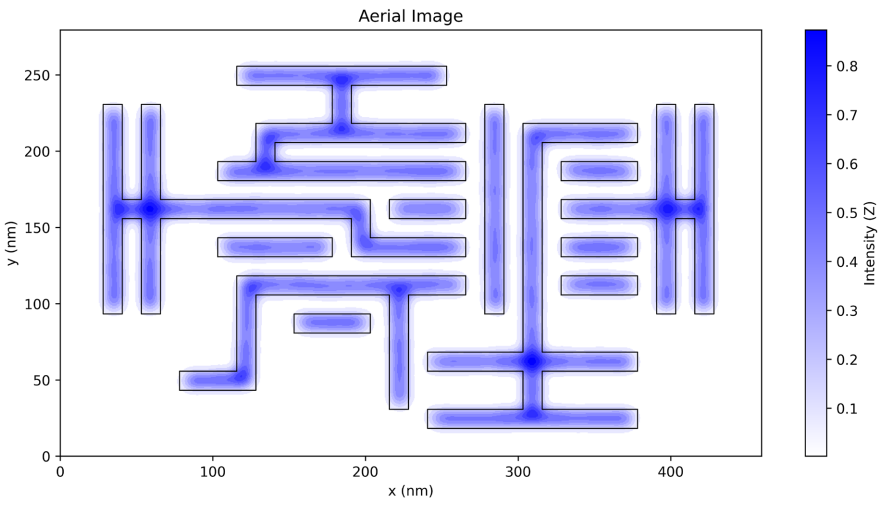

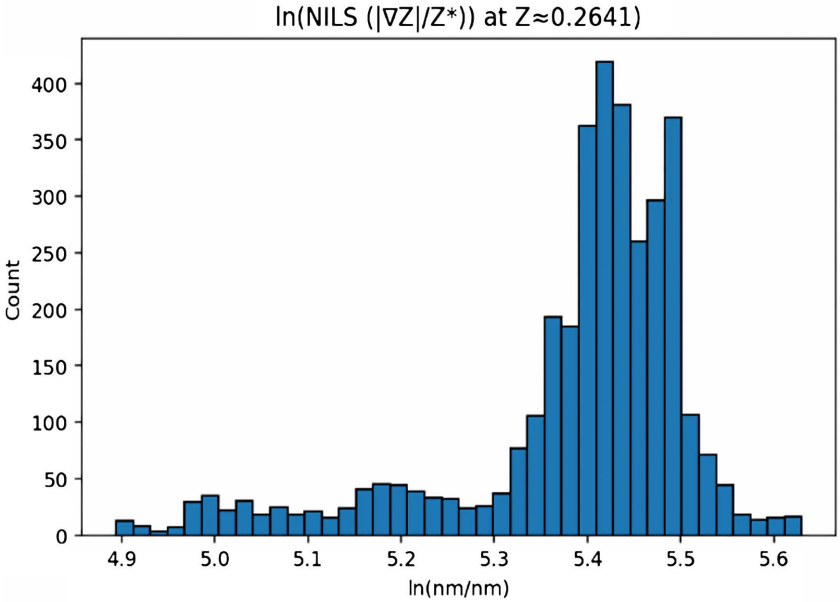

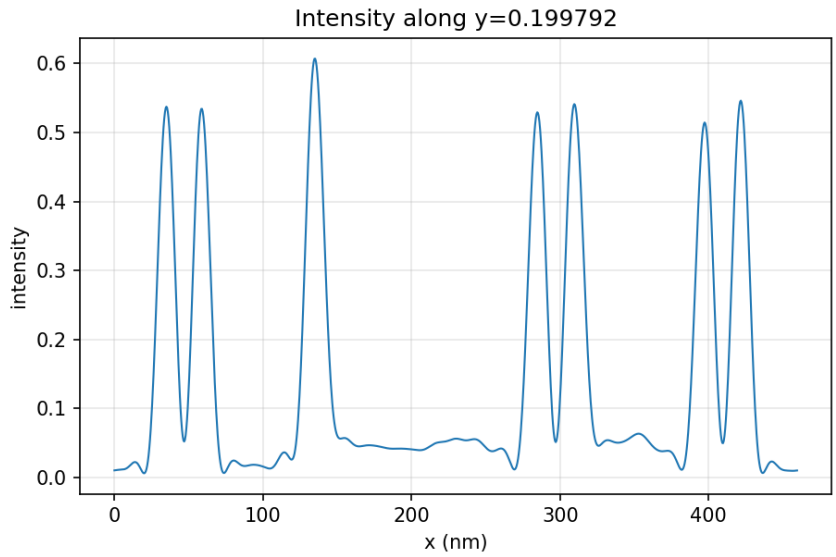

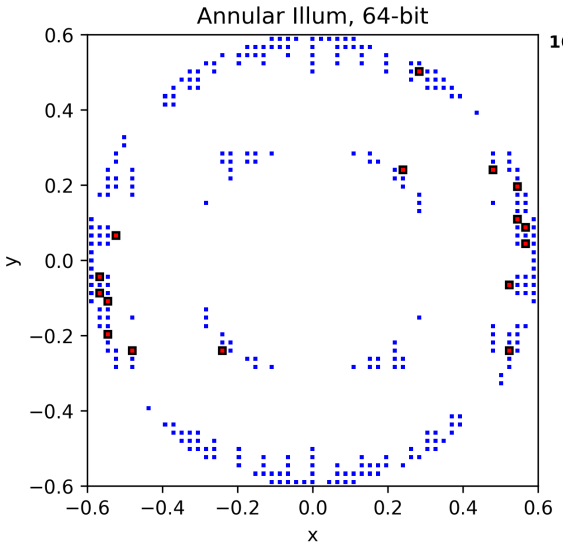

16 Non-binary pixels

x	y	val
0.567	0.0436	0.8713
0.567	0.0873	0.4273
0.545	0.109	0.6959
0.545	0.196	0.8122
0.24	0.24	0.8309
0.48	0.24	0.8949
0.284	0.502	0.4985
-0.524	0.0655	0.8511
-0.48	-0.24	0.8311
-0.24	-0.24	0.4545
-0.545	-0.196	0.8241
-0.545	-0.109	0.7259
-0.567	-0.0873	0.9385
-0.567	-0.0436	0.1134
0.524	-0.24	0.3239
0.524	-0.0655	0.9487

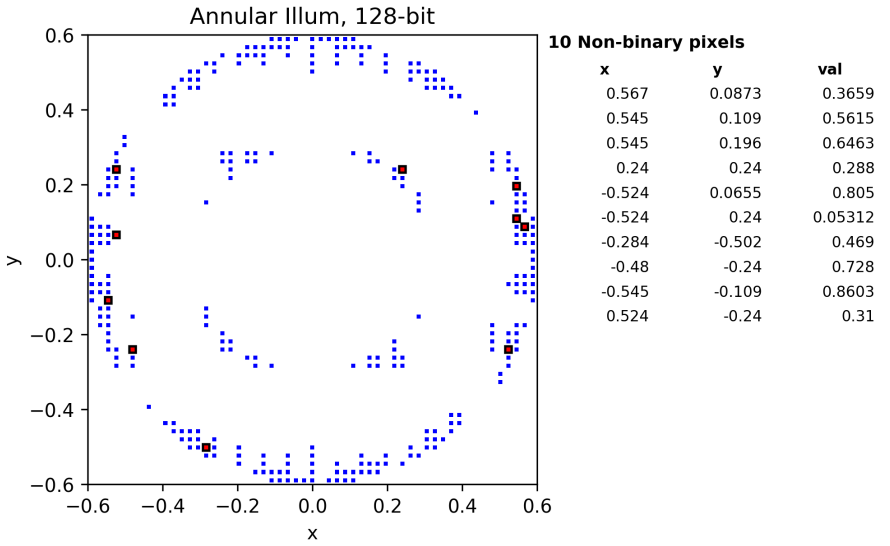

Figure 15. Large arbitrary pattern/circular illuminator; aerial image, NILS histogram, line intensity, and illuminator plots in 64- and 128-bit precision.

4. Conclusion

This study examined why convex QP formulations of pixelated source optimization for EUV lithography routinely produce almost-binary illuminators for most pupil pixels, with only a small subset taking non-binary values. Increasing the total power constraint W systematically reduces the number of non-binary pixels and pushes solutions toward fully binary sources (**Figure 4**). In contrast, changing the measurement pairs can produce abrupt, non-monotonic changes in the non-binary count and quantitatively different illuminator geometries (**Figure 5**, **Figure 6**). Finally, increasing arithmetic precision from 64-bit to 128-bit reduces the non-binary set while leaving the aerial image effectively unchanged (**Figure 7**), indicating that non-binary pixels reflect weakly identified degrees of freedom in the objective rather than meaningful physical structure. Practically, these results imply that residual non-binary pixels should be treated as a numerical symptom of near degeneracy in the QP, not as a requirement for imaging performance. When the objective landscape is nearly flat over a face of the feasible set, multiple illuminators can be essentially equivalent in optimality and ultimately leave the aerial image unaffected.

Conflicts of Interest

The authors declare no conflicts of interest regarding the publication of this paper.

References

[1] Li, Z., Dong, L., Ma, X. and Wei, Y. (2024) Fast Source Mask Co-Optimization Method for High-Na EUV Lithography. *Opto-Electronic Advances*, **7**, 230235. https://doi.org/10.29026/oea.2024.230235

[2] Liu, J., Zhou, J., Sun, H., Jin, C., Wang, J. and Hu, S. (2023) The Inverse Optimization of Lithographic Source and Mask via GA-APSO Hybrid Algorithm. *Photonics*, **10**,

638. https://doi.org/10.3390/photonics10060638

[3] Yang, Y., Liu, K., Gao, Y., Wang, C. and Cao, L. (2025) Advancements and Challenges in Inverse Lithography Technology: A Review of Artificial Intelligence-Based Approaches. *Light*: *Science & Applications*, **14**, 250. https://doi.org/10.1038/s41377-025-01923-w

[4] Yeung, M. and Barouch, E. (2023) Binary Solution for Optimization of Pixelated EUV Source Using Constrained Mathematical Programming. *Optical and EUV Nanolithography XXXVI*, SPIE Advanced Lithography + Patterning, San Jose, California, United States, 26 February-2 March 2023, 124940K. https://doi.org/10.1117/12.2659099

[5] Balay, S., Abhyankar, S., Adams, M.F., Benson, S., Brown, J., Brune, P., *et al.* (2025) PETSc/TAO Users Manual (ANL-21/39, Revision 3.24). Argonne National Laboratory.

[6] Nakata, M. (2010) The MPACK (MBLAS/MLAPACK): A Multiple Precision Arithmetic Version of BLAS and LAPACK (Version 0.6.7). Computer Software. http://mplapack.sourceforge.net/